

Ribonuclease inhibitor 1 regulates erythropoiesis by controlling GATA1 mRNA translation

Vijaykumar Chennupati, ... , Trang Hoang, Ramanjaneyulu Allam

J Clin Invest. 2018. <https://doi.org/10.1172/JCI94956>.

Research Article In-Press Preview Development Hematology

Ribosomal proteins (RP) regulate specific gene expression by selectively translating subsets of mRNAs. Indeed, in Diamond–Blackfan anaemia and 5q- syndrome, mutations in RP genes lead to a specific defect in erythroid gene translation and cause anaemia. Little is known about the molecular mechanisms of selective mRNA translation and involvement of ribosomal-associated factors in this process. Ribonuclease inhibitor (RNH1) is an ubiquitously expressed protein that binds to and inhibits pancreatic-type ribonucleases. Here we report that RNH1 binds to ribosomes and regulates erythropoiesis by controlling translation of the erythroid transcription factor GATA1. *Rnh1*-deficient mice die between embryonic days E8.5 to E10 due to impaired production of mature erythroid cells from progenitor cells. In *Rnh1*-deficient embryos, mRNA levels of *Gata1* are normal, but GATA1 protein levels are decreased. At the molecular level, we found that RNH1 binds to the 40S subunit of ribosomes and facilitates polysome formation on *Gata1* mRNA to confer transcript-specific translation. Further, RNH1 knock down in human CD34⁺ progenitor cells decreased erythroid differentiation without affecting myelopoiesis. Our results reveal an unsuspected role for RNH1 in the control of GATA1 mRNA translation and erythropoiesis.

Find the latest version:

<https://jci.me/94956/pdf>



Ribonuclease Inhibitor 1 regulates erythropoiesis by controlling GATA1 translation

Vijaykumar Chennupati^{1,15}, Diogo F.T. Veiga^{2,13,15}, Kendle M. Maslowski^{3,14,15}, Nicola Andina^{4,5,15}, Aubry Tardivel^{3,4,5}, Eric Chi-Wang Yu³, Martina Stilinovic^{4,5,6}, Cedric Simillion^{5,7}, Michel A. Duchosal⁸, Manfredo Quadroni⁹, Irene Roberts¹⁰, Vijay G Sankaran^{11,12}, H. Robson MacDonald¹, Nicolas Fasel³, Anne Angelillo-Scherrer^{4,5}, Pascal Schneider^{3,15}, Trang Hoang^{2,15}, Ramanjaneyulu Allam^{4,5}

1. Ludwig Center for Cancer Research, University of Lausanne, CH-1066 Epalinges, Switzerland
2. Institute of Research in Immunology and Cancer, University of Montreal, Montréal, Québec H3C 3J7, Canada
3. Department of Biochemistry, University of Lausanne, CH-1066 Epalinges, Switzerland
4. Department of Hematology, Inselspital, Bern University Hospital, University of Bern, Switzerland
5. Department of BioMedical Research, University of Bern, Switzerland
6. Graduate school of Biomedical science, University of Bern, Bern, Switzerland
7. Interfaculty Bioinformatics Unit, University of Bern, 3008 Bern, Switzerland
8. Service and Central Laboratory of Hematology, CHUV, University Hospital of Lausanne, CH-1011 Lausanne, Switzerland
9. Protein Analysis Facility, University of Lausanne, CH-1015 Lausanne, Switzerland
10. Department of Paediatrics and MRC Molecular Haematology Unit, Oxford University; Weatherall Institute of Molecular Medicine, John Radcliffe Hospital, Oxford, OX3 9DU, UK.
11. Division of Hematology/Oncology, Boston Children's Hospital and Department of Pediatric Oncology, Dana-Farber Cancer Institute, Harvard Medical School, Boston, MA 02115, USA.
12. Broad Institute of MIT and Harvard, Cambridge, Massachusetts, USA.
13. Present affiliation: The Jackson Laboratory for Genomic Medicine - Farmington, CT USA
14. Present affiliation: Institute of Immunology and Immunotherapy and Institute of Metabolism and Systems Research, College of Medical and Dental Sciences, University of Birmingham, UK
15. Contributed equally

Correspondence: Ramanjaneyulu Allam, Department of Hematology, Inselspital, Bern University Hospital, University of Bern, Murtenstrasse 40, CH-3008 Bern. Switzerland. Phone: +41-31 632 7753
Email: allam.ramanjaneyulu@dbmr.unibe.ch
orcid.org/0000-0002-2789-3596

Conflict of interest statement: The authors have declared that no conflict of interest exists.

ABSTRACT

Ribosomal proteins (RP) regulate specific gene expression by selectively translating subsets of mRNAs. Indeed, in Diamond–Blackfan anaemia and 5q-syndrome, mutations in RP genes lead to a specific defect in erythroid gene translation and cause anaemia. Little is known about the molecular mechanisms of selective mRNA translation and involvement of ribosomal-associated factors in this process. Ribonuclease inhibitor (RNH1) is an ubiquitously expressed protein that binds to and inhibits pancreatic-type ribonucleases. Here we report that RNH1 binds to ribosomes and regulates erythropoiesis by controlling translation of the erythroid transcription factor GATA1. *Rnh1*-deficient mice die between embryonic days E8.5 to E10 due to impaired production of mature erythroid cells from progenitor cells. In *Rnh1*-deficient embryos, mRNA levels of *Gata1* are normal, but GATA1 protein levels are decreased. At the molecular level, we found that RNH1 binds to the 40S subunit of ribosomes and facilitates polysome formation on *Gata1* mRNA to confer transcript-specific translation. Further, RNH1 knock down in human CD34+ progenitor cells decreased erythroid differentiation without affecting myelopoiesis. Our results reveal an unsuspected role for RNH1 in the control of GATA1 mRNA translation and erythropoiesis.

INTRODUCTION

Regulation of gene expression is important for normal development. Recent studies show that ribosomal proteins regulate gene expression by selectively facilitating translation of specific mRNAs (1, 2). For example, RPL38 specifically enhances translation of a subset of Hox mRNAs (3). Mutations in ribosomal proteins impair ribosome function and cause macrocytic anemia in Diamond–Blackfan anemia (DBA), a congenital bone marrow failure syndrome, and in the 5q- syndrome, a subtype of myelodysplastic syndrome (4). Surprisingly, the majority of clinical symptoms are related to erythropoiesis. In support of these observations, ribosomal deficiencies in DBA impair translation of transcripts essential for erythroid differentiation (5, 6). How ribosomal proteins regulate specific gene expression and how mutations in ribosomal proteins lead to tissue-specific phenotypes is an area of active investigation.

Ribonuclease Inhibitor (RNH1 also known as RI) is a ubiquitously expressed 50 kDa leucine-rich repeat (LRR) protein (7). It is mainly localized in the cytosol, but can also be found in the nucleus and mitochondria (8). RNH1 was the first LRR protein to be crystallized, revealing a horseshoe-shaped three-dimensional structure (9). The human *RNH1* gene evolved via gene duplication and is conserved among mammalian species with human, porcine, mouse, and rat RNH1 proteins sharing 66% identity (10).

Multiple biological roles have been proposed for RNH1. It binds to and inhibits ribonucleases such as RNase A, RNase 1, eosinophil-derived neurotoxin (EDN, also known as RNase 2) and RNase 4 (7). RNH1 affinity for ribonucleases is the key determinant factor for RNase cytotoxicity; only ribonucleases that evade RNH1 can

kill a cell. RNH1 also binds to angiogenin (ANG), suggesting a possible role in neovascularization (11), but the extent to which RNH1 may regulate angiogenesis remains unclear. Further, RNH1 contains numerous cysteine residues (*e.g.* 32 in human RNH1) whose sulfhydryl groups might play key structural roles and protect from oxidative damage (7, 12). There are several conflicting reports about the role of *RNH1*. For example, siRNA knockdown of *RNH1* does not sensitize cells to non-cytotoxic RNases and its role in oxidative damage is not firmly established (7, 8, 12, 13). However, despite these observations, the physiological functions of RNH1 remain unexplored.

In this study, we describe an unsuspected role for RNH1 in embryonic erythropoiesis and erythroid differentiation. We find that RNH1 is a ribosomal associated protein that regulates erythropoiesis by controlling translation of the erythroid transcription factor GATA1. Like *Gata1*-deficient mice, *Rnh1*-deficient mice die from anemia *in utero*.

RESULTS

Embryonic lethality in *Rnh1*-deficient mice

To gain insight into the biological function of RNH1, *Rnh1*-deficient (*Rnh1*^{-/-}) mice were generated through homologous recombination (**Figure. 1, A and B**). When *Rnh1* heterozygous (*Rnh1*^{+/-}) mice were intercrossed, both *Rnh1*^{+/+} (n = 77) and *Rnh1*^{+/-} (n = 151) mice were observed at the expected 1:2 ratio, but *Rnh1*^{-/-} mice were strikingly absent (**Table. 1**). Similar results were also found in Neo cassette-deleted *Rnh1*^{-/-} mice (data not shown). We next examined embryonic development and found that *Rnh1*^{-/-} embryos developed normally before embryonic day 7.25 (E7.25) (**Supplemental Figure. 1A**) but showed an overall growth retardation between E8.5 to E10, with a severe decrease in blood levels in the yolk sac and in the embryo proper (**Figure. 2A, B and Supplemental Figure. 1B and Table. 1**). At this time point, major developmental features such as chorio-allantoic fusion, rotation of the embryo, neural tube closure and formation of head structures were present. The complete absence of viable embryos after E10.5 indicated an essential role for *Rnh1* during this developmental window.

Defective embryonic erythropoiesis in *Rnh1*-deficient mice

Histological examination revealed a profound decrease of erythroid cells in yolk sac blood islands (**Figure. 2C**) and in the placenta (**Figure. 2D**). In addition, the few erythroid cells in yolk sac blood islands of *Rnh1*^{-/-} embryos showed reduced staining with the heme-specific dye benzidine, indicative of a reduced load of haemoglobin (**Figure. 2E**). Endothelium-lined blood vessels were however similar in *Rnh1*^{+/-} and

Rnh1^{-/-} yolk sacs (**Figure. 2C**), and other tissues of mesodermal origin such as somites and myocardium were present (**Supplemental Figure. 1, C and D**). We confirmed that *Rnh1* mRNA was absent in the yolk sac of *Rnh1*^{-/-} embryos (**Figure. 2F**). Since compromised vasculogenesis could affect embryonic erythropoiesis (14), we checked blood vessel formation in *Rnh1*^{-/-} embryo by immunostaining with Pecam-1 (CD31) and by flow cytometry. Blood vessel formation was intact in *Rnh1*^{-/-} embryos as judged by Pecam-1 (CD31) immunostaining (**Figure. 2H**). Similar percentages of CD31⁺ cells were also detected by flow cytometry in all genotypes with a moderate increase in *Rnh1*^{-/-} yolk sacs (**Figure. 2G**). Therefore, anemia was not associated with defective vasculogenesis. During development, the endothelial and hematopoietic lineages originate from a common precursor, the hemangioblast (15). The presence of Pecam-1⁺ endothelial cells in *Rnh1*^{-/-} embryos indicates that hemangioblasts were produced in these embryos, and that the defect was hematopoietic-specific.

The first wave of hematopoiesis is transient and takes place in the yolk sac, giving rise to a single lineage-restricted population of embryonic primitive erythroid cells (EryP) (16). In both humans and mice, yolk sac-derived EryP support the rapid growth of the embryo during early embryonic development (17). Our observations so far are consistent with the view that embryonic death may be attributed to severely decreased blood cell formation and anemia. Interestingly, the phenotype of *Rnh1*-deficient embryo is similar to those of *Gata1*- and *Gata2*-deficient embryos (18). Nonetheless, mRNA levels of *Gata1* and *Tal1/SCL*, two transcription factors that are essential for embryonic erythropoiesis (19, 20), were not affected (**Figure. 2I**) despite reduced erythroid cells in the *Rnh1*^{-/-} yolk sac (**Figure. 2C**). α -fetoprotein (*Afp*), the fetal equivalent of serum albumin, was also similarly expressed in *Rnh1*^{+/+} and *Rnh1*^{-/-}

(**Figure. 2I**). We also assessed the ability of E8-9.5 yolk sac-derived cells to form erythroid colonies using a methylcellulose colony-forming assay. In comparison to *Rnh1*^{+/+} and *Rnh1*^{+/-}, the number of *Rnh1*^{-/-} colonies was significantly decreased (**Figure. 2J**). Control yolk sac colonies displayed a BFU-E (erythroid burst forming units)-like morphology, and contained erythroid cells. *Rnh1*^{-/-} yolk sac colonies had a similar morphology, but with pale colour and contained less mature erythroid cells (**Supplemental Figure. 2A and B**). FACS analysis of colony cells revealed that Ter119 and CD71 (transferrin receptor 1)-positive erythroid cells could develop from *Rnh1*-deficient progenitors, but with a markedly decreased frequency compared to *Rnh1*-proficient cells (**Supplemental Figure. 2C**). These data suggest that an intrinsic differentiation defect of progenitor cells precedes the appearance of anemia and the growth defect phenotype. Although the onset of erythropoiesis can occur in *Rnh1*^{-/-} embryos, it is profoundly decreased.

***Rnh1* expression during embryonic development**

In the adult, *Rnh1* is expressed ubiquitously. However, *Rnh1* expression during embryonic development has not been investigated. *Rnh1* expression increased from E8 to E9.5 (**Figure. 3A**) and, at E9.5, was 7-fold higher in the yolk sac compared to the embryo proper (**Figure. 3B**), coinciding with the site of primitive erythropoiesis (17). It has been reported that RNH1 is highly expressed in erythrocytes (21). We indeed found co-localization of immunostainings for RNH1 and Ter119, a marker of erythroid cells, in the yolk sac and embryo proper of E10.5 wild type embryos, in line with a role for RNH1 in embryonic erythropoiesis (**Figure. 3C and Supplemental Figure. 3**). High expression of the *Rnh1* gene in Ter119⁺ erythroid cells during embryonic development concurs with a role for *Rnh1* in embryonic erythropoiesis.

***Rnh1* regulates erythroid differentiation**

Hematopoietic stem/progenitor cells (HSPCs) that give rise to primitive hematopoiesis are highly enriched in the population of c-Kit⁺CD41⁺ cells from the yolk sac (22-24). These cells are transient progenitor populations distinct from later HSC populations that emerge. FACS analysis revealed that the percentage of c-Kit⁺CD41⁺ (HSPC) cells present in yolk sacs was comparable in all genotypes (**Figure. 3D**). This observation excludes the possibility that the phenotype of *Rnh1*-deficient embryos may result from defects in HSPC generation. The paucity of nucleated erythroid cells in blood islands of *Rnh1*-deficient yolk sacs (**Figure. 2C**) led us to analyze E8.5 and E9.5 yolk sac cells by flow cytometry for the erythroid markers Ter119 and CD71. This analysis revealed that EryP cells (Ter119⁺ and CD71⁺) were significantly decreased in *Rnh1*-deficient yolk sacs (**Figure. 3E**), while HSPCs were not affected (**Figure. 3D**). We also found more binucleated erythroblast in *Rnh1*^{-/-} yolk sac (**Figure. 3F**), indicating an ineffective erythropoiesis. Together, these data suggest that *Rnh1* is required for efficient differentiation of HSPCs into EryP cells, a process essential for embryonic growth and survival. Since colony assays are based on the capacity of these progenitors to give rise to erythroid cells *in vitro*, these observations explain why colony numbers are decreased (**Figure. 2J**) but not the actual frequency of HSPCs.

Decreased splenic erythropoiesis in *Rnh1*^{+/-} adult mice

Heterozygous (*Rnh1*^{+/-}) mice survive normally and did not show any phenotypic abnormalities, suggesting that one allele of *Rnh1* is sufficient for its function. Because our results suggest that *Rnh1* regulates erythroid differentiation, we checked whether

Rnh1 haploinsufficiency decreased adult erythropoiesis. While there was no difference in erythroid cell numbers in *Rnh1*^{+/-} bone marrow (BM) compared to wild type littermates (**Figure. 4, A and B**), erythroid cells in the spleen were significantly decreased (**Figure. 4, C and D**). All four erythroid subpopulations, distinguished by differential expression of Ter119 and CD71 (25), were decreased in *Rnh1*^{+/-} spleen compared to *Rnh1*^{+/+} (**Figure. 4, C and D**). Further, FACS forward scatter (indicator of cell size) was also increased in *Rnh1*^{+/-} erythroid cells, indicating decreased erythroblast maturation (25) (**Figure. 4E**). In contrast, there was no difference in numbers of T cells, B cells and macrophages in the spleen (**Figure. 4 F**). Therefore, *Rnh1* is haplo-insufficient for erythropoiesis in the spleen, further pointing to the importance of *Rnh1* in maintaining erythropoiesis.

RNH1 deficiency decreases *Gata1* mRNA translation

To get clues on the mechanism(s) causing decreased erythropoiesis in *Rnh1*^{-/-} embryos, we performed a transcriptome analysis on *Rnh1*^{+/+}, *Rnh1*^{+/-} and *Rnh1*^{-/-} yolk sac. There was no change between *Rnh1*^{+/+} and *Rnh1*^{+/-} gene expression patterns (GEO, GSE48146), but 628 genes were significantly lower, including genes of mature erythrocytes and genes involved in erythrocyte differentiation, while 273 genes were more expressed in *Rnh1*^{-/-} compared to *Rnh1*^{+/+} (**Figure. 5A and Supplemental Table. 1**). A phenotype enrichment analysis revealed hematopoietic defects such as abnormal blood coagulation, hemostasis and erythrocyte physiology, as main gene signatures among down-regulated genes, in tight agreement with hematopoiesis and erythroid differentiation defects observed in *Rnh1*^{-/-} mice (**Supplemental Figure. 4A and Supplemental Table. 2**).

Several transcription factors are required for erythropoiesis. We applied gene set enrichment analysis (GSEA) in a large dataset of ChIP-seq studies to find out whether targets of hematopoietic transcription factors were differentially regulated in the transcriptome of *Rnh1*^{-/-} yolk sacs (see **Methods**). GSEA scores for most tested regulators, including essential erythropoietic regulators such as GATA1, LDB1, TAL1 and PPARG, were remarkably similar, indicating that their target genes were less expressed in the *Rnh1*^{-/-} yolk sac (**Figure. 5B** and **Supplemental Figure. 4B** and **Supplemental Table. 3**). This global down regulation of hematopoietic TF target genes, but not the TFs themselves, suggests that a post-transcriptional mechanism affects TF gene function, particularly in the erythroid lineage. In support of this hypothesis, a western blot analysis performed on total *Rnh1*-deficient embryos revealed decreased protein levels of GATA1 (**Figure. 5C**). We focused on GATA1 because it was top ranked by GSEA analysis and because it is an important hematopoietic TF, without which erythropoiesis does not take place at all developmental stages in mice and humans (26, 27). The deficit in GATA1 was not only the mere result of a reduced number of erythroid cells in *Rnh1*^{-/-} embryos since mRNA levels were not diminished to the same degree, as witnessed by a markedly decreased protein-to-mRNA ratio (**Figure. 5, D and E**). To check whether decreased GATA1 protein levels reflected impaired translation, we profiled polysomes extracted from yolk sac cells. mRNA contained in polysomes are bound to multiple ribosome units and actively translated; thus, the measure of polysome-associated mRNAs is an indication of their translation rate (3). Polysomes were decreased in *Rnh1*^{-/-} cells and, when normalized to 18S rRNA, polysome and monosome fractions contained lower levels of *Gata1* mRNA than those of *Rnh*^{+/-}, while mRNA levels of another erythroid

TF, *Hoxb4*, remained comparable in *Rnh1*^{-/-} and *Rnh1*^{+/-} polysomes (**Figure. 5, F and G**). These results suggest that even though the overall translation rate is affected in *Rnh1*^{-/-} cells, *Gata1* mRNA translation is further specifically decreased. Global protein levels were comparable in E10 embryos as seen with ponceau S staining (**Figure. 5C**) and also CD31 levels were not decreased in *Rnh1*^{-/-} endothelial cells (**Figure. 2H**). A specific decrease of *Gata1* mRNA translation was also observed in cells deficient for ribosomal protein RPS19, which is mutated in DBA patients (6). In support of an upstream role of RNH1 in GATA1 expression, transient expression of GATA1 in yolk sac *Rnh1*^{-/-} cells restored the usual frequency of erythroid colonies in a methylcellulose colony-forming assay (**Figure. 6, A and B and Supplemental Figure. 5**). Taken together, these results suggest that RNH1 is required for efficient recruitment of *Gata1* mRNA to the ribosome complex.

RNH1 regulates erythroid differentiation by controlling GATA1 translation in human erythroleukemia K562 cells

We wanted to confirm some of the results obtained in *Rnh1*-deficient mice using a human cell line. For this purpose, we knocked-out *RNH1* using the CRISPR/cas9 system in the erythroleukemia cell line K562, which expresses embryonic globin genes (28) (**Figure. 7A**), and indeed reproduced many of the findings obtained in *Rnh1*^{-/-} mice: *RNH1*-KO cells expressed less GATA1 protein compared to wild type cells, even though *GATA1* mRNA levels were similar (**Figure. 7, A and B**). The percentage of benzidine-positive cells was decreased in unstimulated *RNH1*-KO cells (**Figure. 7C**) and in hemin-treated cells (**Figure. 7D**), suggesting a defect in erythroid differentiation. We also found less polysomes in *RNH1*-KO cells (**Figure. 7E**) and decreased *GATA1* mRNA abundance in monosome and polysome fractions compared

to other investigated erythroid genes (**Figure. 7F**). When cells were labelled for 4 h with the methionine analogue L-azidohomoalanine (6), less label was incorporated into GATA1 immunoprecipitates from *RNHI*-KO K562 cells than from control cells, further suggesting that GATA1 translation is impaired in the absence of RNH1 (**Supplemental Figure. 6, A-C**). Furthermore, an RNA-seq analysis showed significant down-regulation of GATA1 target genes in *RNHI*-KO cells compared to wild type (**Supplemental Figure. 7** and **Supplemental Table. 4**). Finally, transient expression of GATA1 in *RNHI*-KO cells restored the usual frequency of benzidine-positive cells, in line with a role of RNH1 upstream of GATA1 expression (**Supplemental Figure. 8**). Moreover, over-expression of Flag-RNH1 in wild type K562 cells increased the relative abundance of polysomes, increased globin mRNA levels and increased the percentage of benzidine-positive cells (**Figure. 8, A-E**), further indicating that RNH1 is functional in human K562 cells in a cell-intrinsic manner.

RNH1 is known to inhibit ribonucleases and protect RNA, raising the question of whether this function might contribute to decrease or increase polysomes in *RNHI*-deficient or overexpressing cells, respectively. To address this, we checked 28S/18S rRNA ratio and RNA quality, and found that both were comparable in RNH1-KO and wild type K562 cells (**Supplemental Figure. 9, A and B**). Further, overexpression an RNH1-mutant (RNH1 Δ C) that does not bind to RNase1 also increased polysomes (**Supplemental Figure. 10, A-C**). These results suggest that polysome stabilization by RNH1 might be independent of its RNase inhibitor function. A recent study has suggested that GATA1-mutant human erythroid cells in culture failed to upregulate expression of translation apparatus genes (29). In K562 cells, however, ribosome

biogenesis and rRNA processing genes were not reduced in the absence of RNH1 (**Supplemental Figure. 11, A and B**). Overall, these results suggest that RNH1 controls GATA1 translation.

RNH1 regulates erythroid differentiation in primary human CD34+ HSPCs

We evaluated whether RNH1 also regulates differentiation of primary adult human CD34+ hematopoietic stem and progenitor cells (HSPC) to the erythroid lineage. In these cells, RNH1 was knocked down using short hairpin RNAs (shRNAs) and erythroid and myeloid differentiation was induced separately as shown schematically in **Figure. 9A**. RNH1 knock down efficiently decreased RNH1 protein levels in CD34+ HSPCs (**Figure. 9B**). Surface expression of CD71 (loss of CD71 indicates erythroid maturation) remained high in RNH1 knock down cells (**Figure. 9C and Supplemental Figure. 12**), suggesting decreased erythroid maturation. RNH1 knock down cells also showed decreased enucleation as determined by Hoechst 33342 staining (**Figure. 9D**). Further, morphological analysis of cytopins showed decreased maturation and enucleation in RNH1 knockdown cells (**Figure. 9 F**). However, there was no difference in myelopoiesis as determined by CD16/CD11b FACS staining and in mature neutrophil numbers (**Figure. 9 E and F**). In differentiated myeloid cells, RNH1 knock down did not affect mRNA and protein levels of the myeloid transcription factors PU.1(SPI1) and C/EBP α (CEBPA) (**Figure. 9 G and H**). In contrast, GATA1 protein, but not mRNA levels were decreased in erythroid cells knocked down for RNH1 (**Figure. 9 I and J**). These results support our previous findings in mice and in human K562 cells that RNH1 controls GATA1 translation and erythroid differentiation.

Interestingly, we also observed decreased protein levels of other erythroid transcription factors, FOG1 (ZFPM1) and KLF1, in RNH1 knock down cells (**Figure. 9 J and K**). mRNA levels of *KLF1* were decreased in RNH1 knockdown cells (**Figure. 9 I**). Since GATA1 directly controls KLF1 expression (30, 31), the reduction in GATA1 levels may explain decreased mRNA and protein levels of KLF1. In the case of FOG1, similar to GATA1, mRNA levels were not decreased in RNH1 knockdown cells, suggest that RNH1 might also control FOG1 translation. Overall these results suggest that RNH1 regulates erythropoiesis and can control GATA1 translation in human CD34+ progenitors. RNH1 may also control translation of other genes which affect erythropoiesis.

RNH1 is present in ribosome fractions and binds to small ribosomal subunit

We next wondered how RNH1 was molecularly connected to the translation machinery. In K562 lysates, although the majority of RNH1 was found in a post-ribosomal fraction (S100), RNH1 was also detected in a polysome-enriched fraction (P100) (**Figure. 10A**) and in the polysome fractions of a sucrose gradient (**Figure. 10B**). After high salt (0.5M KCl) treatment, some RNH1 remained associated with the 80S monosome fraction (**Figure. 10C**), while after puromycin-induced dissociation of ribosomes into 40S and 60S subunits (32), RNH1 was found associated to the 40S subunit (**Figure. 10D**). The salt conditions used in this experiment are known to remove translation factors that associate with ribosomes, aminoacyl-tRNA synthetases, and some protein kinases, but not intrinsic ribosomal proteins (32). These results suggest that RNH1 can directly interact with the small ribosomal subunit. In order to confirm the interaction of RNH1 with ribosomes, Flag-RNH1 was immunoprecipitated from transfected or untransfected K562 cells and interacting

proteins were identified by mass spectrometry (**Supplemental Table. 5**). Ribosomal proteins and proteins involved in RNA processing were among the top enriched functional categories that bound to RNH1 (**Figure. 11A**). This was confirmed by western blot for ribosomal proteins RPL11 and RPS3, while two proteins not found in the mass spectrometry analysis, the ribosome protein RPS6 and the elongation factor EEF2, were negative by western blot in the Flag-RNH1 immunoprecipitate (**Figure. 11B**). Further supporting this data, RNH1 was present in a recently analysed mammalian riboproteome (33). Collectively, these results indicate that RNH1 interacts with ribosomal proteins and support the role of RNH1 in translation and erythropoiesis.

DISCUSSION

RNH1 is known to inhibit ribonucleases and protect RNA from degradation. However, the precise biological role of RNH1 *in vivo* remains unexplored. Our results have uncovered a crucial function for RNH1 in the regulation of erythropoiesis by controlling GATA1 translation. Embryonic erythropoiesis starts between E7 to E7.5 by producing primitive erythroid cells from a transient wave of committed progenitors in the yolk sac (16). These primitive erythroid cells support the rapid growth of the embryo during early embryonic development. We demonstrate that *Rnh1* expression localizes to erythroid cells at the onset of primitive erythropoiesis and that *Rnh1* deficiency resulted in a lethal decrease in erythroid differentiation and the hemoglobin content per cell. The anemia phenotype observed in *Rnh1*^{-/-} embryos was not associated with defective vasculogenesis and HSPC generation, since blood vessel formation and HSPC generation was intact. Further, *Rnh1* haploinsufficiency decreased adult erythropoiesis in the spleen, further pointing to the importance of *Rnh1* in maintaining erythropoiesis.

Similarly, RNH1 deficiency in human K562 cells and RNH1 knock down in primary CD34⁺ HSPCs reduced erythroid differentiation, suggesting that its role is conserved across species and that it can play a cell intrinsic function. Interestingly, the transcriptome of *Rnh1*^{-/-} yolk sac cells revealed that the expression levels of erythroid transcription factors were not deficient, but that their target genes were reduced. This is in line with our observation that RNH1 associates with ribosomal proteins to favour polysome formation and enhance translation. Supporting this *GATA1* mRNA levels were not affected but protein levels were decreased. Further, transient expression of GATA1 in RNH1-deficient mouse yolk sac cells and K562 cells restored the

erythroid differentiation defect observed in *RNH1*-deficient cells, suggesting a role of RNH1 upstream of GATA1 expression.

Mutations in ribosomal proteins interfere with ribosome biogenesis, which is considered as the main pathological mechanism for Diamond Blackfan Anaemia (DBA) (4). DBA is a rare congenital pure red cell aplasia characterized by anemia, macrocytosis and reticulocytopenia (4). In DBA patients, mutation of ribosomal proteins, such as RPS19, leads to impaired ribosomal biogenesis and cause a defect in translation of GATA1 and erythroid-related genes (5, 6). Similarly, RNH1 is a ribosome-associated protein expressed by erythroid cells, and whose deficiency causes decreased GATA1 translation and defective differentiation of erythroid cells (**Figure. 12**). Defects in ribosomal biogenesis can lead to TP53 upregulation and apoptosis (34). Nonetheless, impaired erythropoiesis in *Rnh1*-deficient embryos was not associated with p53-dependent apoptosis since we did not find TP53 upregulation nor enrichment of TP53 related apoptotic genes (**Supplementary Table 1**). Although this work focused mainly on GATA1, we consider it likely that RNH1 regulates translation of other erythroid-specific genes. How this specific regulation of translation precisely takes place requires further investigation. RNH1 is only present in vertebrates and was proposed to be an intracellular sentry since it protects cytosolic RNA from extracellular ribonucleases (35). However, our combined functional and systems-level analyses show that this is not the sole, or perhaps even the main function of RNH1 *in vivo*. In conclusion, we present a novel function for RNH1 in GATA1 translation and erythropoiesis. This data adds RNH1 to the list of ribosomal-associated factors that regulate specific mRNA translation (1). This warrants further studies on RNH1 and may provide novel therapeutic opportunities for erythropoiesis-related disorders.

MATERIALS AND METHODS

Generation of $Rnh1^{-/-}$ Mice

$Rnh1$ targeting vector (**Figure. 1A**) was electroporated into hybrid (C57BL/6x129/SvEv) embryonic stem (ES) cells. Homologous recombinant ES cells were identified by Southern blot analysis and microinjected into blastocysts. Offspring were backcrossed to C57BL/6 mice and germline transmission was confirmed by PCR of tail genomic DNA. Screening of $Rnh1$ -deficient mice by PCR genotyping was carried out using the following primers on embryo or ear genomic DNA: 5'CTGATAACTTATTTCCGGG ATAC (forward in intron 1), 5'ACCACTTCGTATTGCTGGA (reverse in exon2) and 5' TAAGCTTGGATCCGTTCTTC (reverse in PGK-NEO cassette). We used 8 weeks-old male $Rnh1^{+/+}$ and $Rnh1^{-/-}$ mice (n = 6 mice) to analyze different cell population in spleen and bone marrow. Mice were handled according to Swiss Federal Veterinary Office guidelines, under valid authorization.

RNA preparation and qRT-PCR

Total RNA was isolated from embryos, yolk sac and K562 cells using Qiagen RNeasy kit according to manufacturer's protocol. Reverse transcription and real time RT-PCR from total RNA was carried out as described previously (36). SYBR Green Dye detection system was used for quantitative real-time PCR on Light Cycler 480 (Roche, Switzerland). Gene-specific primers (Microsynth, Switzerland) were used as listed in **Supplemental Table. 6**. Controls consisting of ddH₂O were negative for target and housekeeper genes.

Gene expression analysis

Total RNA from E9.5 yolk sac of different genotypes (*Rnh1*^{+/+}, *Rnh1*^{+/-} and *Rnh1*^{-/-}) was isolated and purified with Qiagen RNeasy kit according to the manufacturer's protocol. All RNA amounts were monitored with a NanoDrop®ND-1000 spectrophotometer and the RNA quality was assessed using RNA 6000 NanoChips with the Agilent 2100 Bioanalyzer (Agilent, Palo Alto, USA). For each sample, 100 ng of total RNA were amplified using the WT sense strand Target Labelling kit (Affymetrix, Cat.no. 900223); 5.5 µg of the resulting sense cDNA was fragmented by UDG (uracil DNA glycosylase) and APE 1 (apurinic/aprimidic endonuclease 1) and biotin-labelled with TdT (terminal deoxynucleotidyl transferase) using the GeneChip® WT terminal labelling kit (Affymetrix Cat.no. 900671, Santa Clara, USA). Affymetrix Mouse Gene 1.0 ST arrays (Affymetrix, Santa Clara, CA, USA) were hybridized with 2.7 µg of biotinylated target, at 45°C for 17 hours washed and stained according to the protocol described in Affymetrix GeneChip® Expression Analysis Manual (Fluidics protocol FS450_0007). The arrays were scanned using the GeneChip® Scanner 3000 7G (Affymetrix) and raw data was extracted from the scanned images and analysed with the Affymetrix Power Tools software package. Affymetrix Hybridization quality was assessed using the Expression Console software (Affymetrix). Microarray analysis was performed using various Bioconductor packages in the R environment (<http://www.bioconductor.org>). Normalized expression signals were calculated from Affymetrix CEL files using the RMA normalization implemented in the Affy package (37) and differential expression analysis was performed using the Rank Products package (38). Complete microarray datasets are available at GEO under accession number GSE48146.

Phenotype enrichment analysis

We applied the Phenotype Ontology Enrichment available in the MouseMine database (<http://www.mousemine.org>) to determine phenotypes significantly enriched among down-regulated genes in *Rnh1*^{-/-} mice. Enriched phenotypes are related to spontaneous, chemically induced, or targeted mutations of mouse genes. The complete list of significant phenotypes (Benjamini-Hochberg adjusted P-values < 0.05) is found in the **Supplemental Table. 2.**

Target enrichment analysis

The collection of 52 ChIP-seq studies was obtained from the HemoChIP compendium (39). For each ChIP-seq study, we extracted a list of targets by selecting genes containing at least one binding site for the transcription factor in the 2 kb region around the transcription start site. The GSEA test statistic (40) was used to determine up-regulation or down-regulation of transcription factor targets in *Rnh1*^{-/-} mice. Complete GSEA results and target gene sets are available in the **Supplemental Table. 3.**

Hematopoietic colony formation assays

E8, E8.5 and E9.5 yolk sacs were dissected without contamination from maternal tissue under sterile conditions from *Rnh1*^{+/+}, *Rnh1*^{+/-} and *Rnh1*^{-/-} embryos. Cells were isolated from yolk sac by treatment with 0.1% collagenase in PBS and 20% foetal calf serum for 30 minutes at 37°C before mechanical disaggregation as described previously (20). Total yolk sac cells were cultured for 7 days in methylcellulose semi-solid medium containing all essential growth factors that support growth of erythroid progenitors (M3436, Stem Cell Technologies).

Flow cytometry and cell sorting

Single-cell suspensions were prepared from mouse yolk sac and adult bone marrow or spleen. Cells were stained with monoclonal antibodies specific for CD41 (MWReg30), CD117 (2B8), CD31 (390), Ter119 (TER-119), CD71 (R17217), F4/80 (BM8), CD11b (M1/70), CD19 (eBio1D3) and CD3 (17A2). All antibodies were purchased as fluorescein isothiocyanate (FITC), Phycoerythrin (PE), PE-Cy5, PE-Cy7, APC-eFlour780, Alexa Fluor 700, PerCP-eFluor 710 conjugates from eBiosciences. Cells were either acquired on BD LSRII flow cytometer or sorted on FACS Aria I cell sorter (BD Biosciences). Data was analyzed with FlowJo (version 9.3.1, TreeStar Inc) software. For human CD34+ differentiation experiments, cells were stained with anti-human monoclonal antibodies specific for CD11b (ICRF44), CD13 (WM-15), CD16 (eBioCB16), CD71(OKT9), CD235a (HIR2(also GA-R2)). All antibodies were purchased as fluorescein isothiocyanate (FITC), Phycoerythrin (PE), APC from eBiosciences. CD34 (AC136) antibody from Miltenyi Biotec. Hoechst 33342 fluorescent nuclear stain (ImmunoChemistry Technologies) was added at a dilution of 1:200 at least 15 minutes before analysis. Data were acquired on CytoFLEX S Flow Cytometer (Beckman Coulter). Data analysis was carried out with FlowJo 10.2 (FlowJo LLC).

Immunostaining

Embryos were fixed with PFA 4% in PBS for 2 h and then washed with PBST (PBS+ 0.3% Triton X-100). After blocking with 5% donkey serum and 0.5% BSA in PBS, embryos were incubated with primary antibodies in blocking buffer overnight at 4°C. RNH1(Cat no: H00006050-D01P) (Abnova), Ter119 (Cat no:14-5921-82) (eBioscience) and Pecam-1 (Clone: MEC 13.3) (BD Bioscience). After washing

with PBST, embryos were incubated overnight with Alexa Fluor secondary antibodies (Invitrogen) in blocking buffer and rinsed with PBST. Microscopy analyses were carried out using a Leica Stereomicroscope or a Time-Lapse-Inverted microscope (Axio Observer.Z1).

Immunoblotting

Total mouse embryos-derived cells, human K562 cells, CD34+ progenitor cells, erythroid and myeloid cells were resuspended in lysis buffer (20 mM Tris, pH 7.4, 150 mM NaCl, 1% (vol/vol) Nonidet-P40, 10 mM EDTA). Extracts were used for immunoblot. Nitrocellulose membranes were stained with Ponceau S for similar protein loading control. The following antibodies were used: RNH1 (Cat no: H00006050-D01P) from Abnova, Mouse GATA1 (Cat no: Sc-265), RPS3 (Sc-135390) and RPL11 (Sc-25931), human RNH1(sc-365783), human FOG (sc-376189), are from Santa Cruz Biotechnology, Human GATA1 (Cat no: 4591), BCR (Cat no: 3902) and RPS6 (Cat no: 2317), human C/EBPalpha, (Cat no: 2295) anti-human PU.1 (Cat no: 2258), EEF2 (Cat no: 2332) are from Cell signaling, beta-actin (ab8227) human EKLF/KLF1(ab2483) are from Abcam.

Histology

Embryos were embedded in paraffin and sections were used for haematoxylin and eosin staining with routine protocols. Similar sections were used for benzidine staining. Cytospins were prepared from yolk sac cells and stained with Pappenheim stain (May-Grünwald and Giemsa) (Fluka).

CRISPR/CAS9-mediated knockout cell line generation

CRISPR sequences targeting exon 2 (RNH1-KO-1) and exon 3 (RNH1-KO-2) of human RNH1 were designed using the online-available CRISPR design tool developed by the F. Zhang laboratory. The seed sequences preceding the protospacer adjacent motif (PAM) are the following: RNH1-1 oligo 1—5'-*CACCG* CGGCGTGCATTGCGTGCTCC-3'; RNH1-1 oligo 2—5'-*AAACGGAGCACGCAA* TGCACGCCGC-3'; RNH1-2 oligo 1—5'-*CACCGGGGTGCGTAGTGTGCTGGAC*-3'; and RNH1-2 oligo 2—5'-*AAACGTCCAGCACACTACGCACCCC*-3'. Nucleotides in italics show the overhangs necessary for incorporation into the restriction enzymatic site BbsI of LentiCRISPR-v2 vector expressing Cas9 and sgRNA (Adgene #52961) (41). Lentiviruses were produced in 293T cells as previously described (42). K562 cells were infected with lentiCRISPRv2 viruses targeting RNH1-1, RNH1-2 or control. Positive cells were selected with 2 µg/mL puromycin. RNH1 expression was assessed by western blot. To obtain full KO cell lines, population was cloned by limiting dilution and tested again by western blot. All the generated K562 clones were tested negative for mycoplasma contamination using MycoAlert Mycoplasma Detection Kit (Lonza, Cat#LT07-318). K562 cells were from ATCC and authenticated the presence of BCR/ABL fusion gene by western blot (**Figure. 7A**) and cytogenetics (data not shown).

RNA-sequencing and analysis

Total RNA from control K562 and *RNH1*-KO cells was isolated and purified with Qiagen RNeasy kit according to the manufacturer's protocol. We prepared Illumina TruSeq stranded mRNA libraries. The libraries were subjected to a preparative size selection on a PippinHT instrument to exclude library molecules with insert sizes of

less than 300 bp. Libraries were then sequenced with 2 x 150 bp reads on an Illumina HiSeq3000 instrument.

RNA-seq reads were mapped to the human reference genome (GRCh38, build 81) using Tophat v. 2.0.11 (43). We then used HTseq-count v. 0.6.1 (44) to count the number of reads per gene, and DESeq2 v.1.4.5 (45) to test for differential expression between groups of samples. The outcome of the DESeq2 analysis was taken to perform gene set enrichment analysis (GSEA) using the SetRank method (46). This algorithm principally discards gene sets that have initially been flagged as significant, if their significance is merely due to the overlap with another gene set. This method then calculates the P-value of a gene set utilizing the ranking of its genes in the ordered list of P-value as determined by DESeq2. We constructed a gene set database that consisted of the target gene sets of the GATA1 transcription factor. Next, this database was complemented with all pathways that significantly intersect (Fisher's exact test, holm-corrected $p \leq 0.01$) with GATA1 target gene sets. The pathway collections searched came from the following databases: BIOCYC (47), Gene Ontology (48), KEGG (49), Pathway Interaction Database (50), REACTOME(51), and WikiPathways (52). The purpose of adding these additional gene sets is to make sure that the observed significance of the GATA1 target gene set is not purely due to this set intersecting with a more significant pathway. RNA-seq data are available in the ArrayExpress database (www.ebi.ac.uk/arrayexpress) under accession number E-MTAB-5162.

Ribosome profile analysis by sucrose gradient density ultracentrifugation

Yolk sac cells derived from *Rnh1*^{+/-} and *Rnh1*^{-/-} were pooled and cultured for 7 days in methylcellulose semi-solid medium containing all essential growth factors that

support erythroid progenitors (M3436, Stem Cell Technologies) to get enough cells. Approximately 2×10^6 yolk sac-derived cells and 5×10^6 K562 cells were washed with PBS containing cycloheximide (CHX) (100 $\mu\text{g}/\text{ml}$) and resuspended in 200 μl of hypotonic buffer (1.5 mM KCl, 2.5 mM MgCl_2 , and 5.0 mM Tris-Cl, pH 7.4) and 200 μl hypotonic lysis buffer (same with 2% sodium deoxycholate, 2% Triton X-100, and 2.5 mM DTT) + CHX and gently disrupted using a Dounce homogenizer. The lysates were centrifuged at 8,000 g for 10 min at 4°C. The supernatant was supplemented with 80 μl heparin. Linear 10% to 45% sucrose gradients (80 mM NaCl, 5 mM MgCl_2 , 20 mM Tris-Cl, pH 7.4, and 1 mM DTT) were formed manually. Gradients were centrifuged at 36,000 rpm for 3h at 4°C and separated through a live OD254nm ultraviolet spectrometer. All experiments were repeated at least three times in the same conditions.

Protein samples from all fractions were isolated and western blot was performed for RPS3 or RPS6 and RPL11 present in the 40S and 60S subunits, respectively. The monosomes, light and heavy polysomes fractions were determined as reported previously (53). TRIzol Reagent (Invitrogen) was added to each collected fraction and RNA was isolated according to the manufacturer's protocol. Reverse transcription and real time RT-PCR was performed as mentioned previously. 18S rRNA primers were used for normalization of abundance of the mRNA of interest in monosome and polysome gradient fractions. Gene-specific primers (Microsynth, Switzerland) were used as listed in **Supplemental Table. 6**.

Fractionation of ribosome

Polysome-enriched pellet (P100) and a post-polysomal supernatant (S100) were prepared from cytoplasmic extracts as reported previously (32). To completely

dissociate 40S and 60S ribosomal subunits, polysome-enriched pellets were resuspended in a buffer containing 3 mM MgCl₂, 500 mM KCl, and puromycin was added to a final concentration of 1 mM as reported previously (32). Samples were incubated at 37°C for 15 min and centrifuged twice for 15 min at 30,000 g, and the supernatant was loaded on a linear sucrose gradient (10–30%) in the same buffer. The gradients fractions were collected as described above. Following fractionation, proteins were isolated by precipitating with methanol and chloroform method, and western blotted as described above with anti-RPL11, anti-RPS3 (Santa Cruz Biotechnology), anti-RPS6 (Cell Signaling), anti-RNH1 (Abnova).

Generation of RNH1 expression plasmids

The sequence encoding human full-length RNH1 was amplified by PCR and sub-cloned into the mammalian expression vector pCR3 in frame with the N-terminal Flag or VSV tag. Using site-directed mutagenesis kit (Agilent technologies), we generated different RNH1 mutant plasmids and checked their binding with RNase1(54) (See also **Supplemental Figure. 10A**). RNase1 expression plasmid with the C-terminal MYC/Flag tag was purchased from Origene.

Generation of stable K562 cells expressing Flag–RNH1 and RNH1ΔC

Flag-RNH1 or RNH1ΔC was further sub-cloned into retroviral vector pMSCVpuro (Clontech). Retroviral vector pMSCVpuro-Flag-RNH1 or RNH1ΔC was co-transfected with the helper plasmids VSV-G and Hit60 into HEK293T cells using PEI transfection reagent. Culture supernatants containing recombinant viral particles were harvested and used to infect K562 cells. To establish stable cell lines, K562 cells were selected with puromycin (5 μg ml⁻¹) 3 days after infection.

GATA1 rescue experiments

GATA1 expression plasmid was generated as described previously (6). The empty HMD and HMD-GATA1 vectors were transfected with lipofectamine (Invitrogen) in *RNH1*-KO K562 cells and infected with lentivirus vectors in E9.5 *Rnh1*-deficient mice yolk sac cells. 48 h post-transfection or post-infection, transfection or transduction efficiency was monitored by GFP expression (both vectors contain GFP). GFP-positive cells were enriched by FACS sorting and used to perform benzidine staining and western blot with K562 cells. In case of yolk sac cells, GFP-positive cells were cultured for 7 days in methyl cellulose medium which supports erythroid differentiation.

Immunoprecipitation and mass spectrometry analyses

Stable mock- and Flag-RNH1- expressing K562 cells were resuspended in lysis buffer (20 mM Tris, pH 7.4, 150 mM NaCl, 1% (vol/vol) Nonidet-P40, 10 mM EDTA). In other experiments, Flag or VSV tagged constructs and empty vector as shown in (**Supplemental Figure. 10A**) were transfected into HEK293T cells by the calcium-phosphate method. At 24 h after transfection, cells were resuspended in lysis buffer as mentioned above. Extracts were immunoprecipitated with anti-Flag or anti-VSV agarose beads and then were assessed by immunoblot. For mass spectrometry analyses, beads after immunoprecipitation were washed with PBS and resuspended in 1x SDS gel loading buffer to extract bound proteins. Samples were resolved on a 10% mini polyacrylamide gel for about 2 cm, fixed and rapidly stained with Coomassie blue. Entire gel lanes were excised into 5 equal regions from top to bottom and digested with sequencing-grade trypsin (Promega) as described (55). Data-dependent LC-MS/MS analysis of extracted peptide mixtures after digestion was carried out on a

hybrid linear trap LTQ-Orbitrap Velos mass spectrometer (Thermo Fisher Scientific) interfaced via a nanoelectrospray source to a Dionex 3000 RSLC nanoflow UHPLC. Peptides were separated on a Dionex Pepmap C18 (75 μm ID x 250 mm, 2 μm) capillary column (Dionex) along a 90 min gradient from 5 to 85% acetonitrile in 0.1% formic acid at a flow rate of 200 nl min⁻¹. Raw data were used to query a non-redundant protein database using MASCOT software (Matrix Science, London, UK; version 2.4). Functional enrichment analysis was conducted using DAVID bioinformatics tools (<http://david.abcc.ncifcrf.gov/>) (56, 57). Protein interaction networks were visualized using Osprey (58). For immune blot the following antibodies were used. RNH1 (Abnova), RPS3, and RPL11 (Santa Cruz Biotechnology), Flag-Ab (Sigma), RSP6 and EEF2 (Cell Signaling Technology), Beta-Actin (Abcam).

Protein labelling and immunoprecipitation coupled to Click-iT reaction

Click-iT reaction was performed as described previously (6). Briefly, WT and RNH1-KO K562 cells were washed with warm PBS and incubated in methionine-free RPMI medium (R7513, Sigma-Aldrich) with 10% FBS and 2 mM L-glutamine for 1 h at 37°C, 5% CO₂ to deplete methionine reserves. For labeling, Click-iT AHA (l-azidohomoalanine, C10102, Life Technologies) was added at a final concentration of 50 μM for 4 h at 37°C, 5% CO₂. Cells were washed twice in cold PBS and resuspended in lysis buffer (20 mM Tris, pH 7.4, 150 mM NaCl, 1% (vol/vol) Nonidet-P40, 10 mM EDTA) supplemented with protease inhibitor cocktail (S8820-Sigma-Aldrich). Cell lysates were prepared by incubating for 30 min on ice and centrifugation at 13,000 rpm for 10 min at 4°C to remove cellular debris. Using these whole cell lysate, immunoprecipitation was performed with GATA1 antibody (Cat

no: 4591, Cell signaling), bound to Dynabeads Protein G (10003D, Life Technologies) for 3 h with rotation at 4 °C. The antibody-antigen complex was washed three times with lysis buffer and the Click-iT reaction was performed using TAMRA alkyne and the Click-iT Protein Reaction Buffer Kit (C10276, Invitrogen) for 1h at 4 °C according to the manufacturer's instructions. The immunoprecipitate was washed once with lysis buffer, then bound proteins were eluted in SDS sample buffer (3x) by heating at 70 °C for 10 min. Western blot was performed using antibodies against GATA1 or TAMRA (MA1-041, Invitrogen)

Lentiviral production

Lentiviral shRNA plasmids against RNH1 were purchased from Sigma. Lentiviruses for shRNA were produced by cotransfecting HEK293T cells with the shRNA-containing plasmid targeting RNH1 or Scramble (pLKO.1 plasmids: shRNH1—5'-CCG GGC TGG TCC TGT ACG ACA TTT ACT CGA GTA AAT GTC GTA CAG GAC CAG CTT TTT G -3'; 5'; shScramble—5'- CCG GCA ACA AGA TGA AGA GCA CCA ACT CGA GTT GGT GCT CTT CAT CTT GTT GTT TTT-3') plus a lentiviral packaging system (pMD2 VSV and pCMV DR8.91). Cells were transfected using Lipofectamine 2000 transfection reagent (Invitrogen). Supernatant was collected at 72 h post transfection and filtered with a 0.45 mm filter to clear cell debris. 30 ml of virus containing supernatant was collected and passed through a Whatman Puradisc 45 µm filter (GE Healthcare Life Sciences, #6780-2504). After addition of 7.5 ml PBS, 1.3 ml of 5 M NaCl and 8 ml of PEG 8000 solution the mixture was incubated at 4°C on a rotation wheel overnight. PEG 8000 solution was prepared by dissolving 200 g Polyethylene glycol 8000 (Carl Roth, #0263) in 200 ml of PBS, followed by autoclave treatment. The virus was precipitated the next day by

centrifugation at 3220 x g at 4°C for 1 h. The virus-containing pellet was resuspended in PBS and stored at -80°C until use.

Isolation of primary human CD34+ HSPCs

Primary human CD34+ HSPCs were isolated from G-CSF mobilized peripheral blood using CD34 MicroBead Kit (Miltenyi Biotec, #130-046-702) according to the manufacturer's protocol. The purity was assessed by flow cytometry using a PE conjugated anti-human CD34 antibody (Miltenyi Biotec, #130-098-140) and was at least 94%.

Expansion and lentiviral infection of primary human CD34+ HSPCs

After isolation, primary human CD34+ HSPCs were expanded in StemSpan™ SFEM (Stemcell Technologies, #09600) supplemented with StemSpan™ CC100 (Stemcell Technologies, #02690) for 5 days (expansion phase). Lentiviral infection was started on day 2 of the expansion phase for a total of 12 h. For this purpose, cells were cultured at a density of 10⁶ cells/ml. Concentrated virus was added at a ratio of 1:20 and polybrene (Santa Cruz Biotechnology, #sc-134220) at a concentration of 8 µg/ml. Selection was carried out for 30 h after washing by addition of 1 µg/ml puromycin (Sigma-Aldrich, #P9620). After the expansion phase cells were counted and split into two portions. One portion was used for *in vitro* erythroid differentiation, the other one for *in vitro* neutrophilic differentiation.

***In vitro* erythroid differentiation**

In vitro erythroid differentiation was adapted from a previously published protocol (59). In phase 1 (day 0 - 6) cells were cultured at a density of 10⁵ - 10⁶ cells/ml in IMDM (gibco, #21980-032) supplemented with 3% human AB serum and 2% human

AB plasma (Interregional Blood Transfusion SRC, Bern, Switzerland), 1% penicillin/streptomycin (gibco, #15070-063), 3 IU/ml heparin (Sigma-Aldrich, #H3149), 200 µg/ml holo-transferrin (Sigma-Aldrich, #T0665), 10 µg/ml insulin (Sigma-Aldrich, #I3536), 1 IU/ml erythropoietin (PeproTech, #100-64), 10 ng/ml stem cell factor (PeproTech, #300-07) and 1 ng/ml IL-3 (PeproTech, #200-03). In phase 2 (day 6 - 12), IL-3 was omitted.

***In vitro* neutrophilic differentiation**

In vitro neutrophilic differentiation was adapted from a previously published protocol (60). In phase 1 (day 0 - 3) cells were cultured at a density of 10^5 - 10^6 cells/ml in IMDM (gibco, #21980-032) supplemented with 10% foetal calf serum (FCS, Amimed, #2-01F10-I), 1% penicillin/streptomycin (gibco, #15070-063), 100 ng/ml stem cell factor (PeproTech, #300-07) and 100 ng/ml IL-3 (PeproTech, #200-03). In phase 2 (day 3 - 12), G-CSF (PeproTech, #300-23) was supplemented in addition.

May-Grünwald-Giemsa staining

50'000 cells were resuspended in 200 µl culture medium and spun onto a cytospin slide in a Cytospin™ 4 Cytocentrifuge (Thermo Scientific, #A78300003) at 600 rpm for 10 minutes. Slides were air-dried for at least 10 minutes. Slides were then stained in May-Grünwald solution (Merck, #1.01424.2500) for 4 minutes, rinsed in deionized water for 2 minutes, stained in Giemsa solution (Merck, #1.09204.0500) for 14 minutes and rinsed twice in deionized water for 2 and 1 min, respectively. Pictures were taken with a PMW-10MD camera from Sony by using Carl Zeiss, Axioskop 50 microscope

Statistical analysis

Data were expressed as mean \pm SEM or mean \pm SD of at least three biological replicates. Comparison between two groups was performed by two-tailed *t*-test. A value of $p < 0.05$ was considered to be statistically significant. All statistical analyses were calculated using Graph Pad Prism. No statistical methods were used to predetermine sample size. The experiments were not randomized and the investigators were not blinded to allocation during experiments and outcome assessment. Gene expression studies were performed using three independent biological replicates from each genotype, (*Rnh1*^{+/+}, *Rnh1*^{+/-} and *Rnh1*^{-/-}). RNAseq experiments were also performed in triplicates. Mass spectrometry studies were performed once.

Study approval

All animal experiments were approved by the Swiss Federal Veterinary Office, Bern, Switzerland, under valid authorization (BE39/16). Approval for the use of human CD34+ cells obtained from Kantonale Ethikkommission Bern, Switzerland.

Data availability

All datasets generated and analysed during the current study are available in **Supplemental Tables. 1 to 5**. Microarray and RNA-seq data that support the findings of the study have been deposited at the NCBI gene expression omnibus (GEO; www.ncbi.nlm.nih.gov/geo/) with the GEO accession number GSE48146 and RNA-seq data are available in the ArrayExpress database (www.ebi.ac.uk/arrayexpress) under accession number E-MTAB-5162.

Supplementary information included along with this manuscript

ACKNOWLEDGEMENTS

We thank Florence Morgenthaler for microscopy (CIF facility, University of Lausanne); Janine Horlbeck and Jean-Christophe Stehle for histopathology (mouse pathology facility, University of Lausanne); Keith Harshman for micro-array studies (CIG, University of Lausanne). We thank the Next Generation Sequencing (NGS) Platform for RNA-Seq studies (University of Bern). This work was supported by the Swiss National Science Foundation (PP00P3_157486) to RA, the Louis Jeantet Foundation, and the Institute for Arthritis Research. We dedicate this work to the memory of Jürg Tschopp who initiated this project and inspired many of us.

AUTHOR CONTRIBUTIONS

RA designed experiments, performed most experimental work, analysed data and wrote the manuscript. VC, KMM and NA helped with experimental work and writing of the manuscript. DFTV performed microarray-related analyses and helped with writing of the manuscript. AT maintained mouse lines and helped with experimental work. CHY and MS helped with experimental work. CS and MQ generated and analyzed the RNA-seq and mass spec data, respectively. MD, HRM, IR, NF, VGS and AAS provided reagents and critical suggestions. TH and PS helped with the experimental design, analysing the data and writing of the manuscript.

REFERENCES

1. Shi Z, Barna M. Translating the genome in time and space: specialized ribosomes, RNA regulons, and RNA-binding proteins. *Annu. Rev. Cell Dev. Biol.* 2015;31:31–54.
2. Xue S, Barna M. Specialized ribosomes: a new frontier in gene regulation and organismal biology. *Nat. Rev. Mol. Cell Biol.* 2012;13(6):355–369.
3. Kondrashov N et al. Ribosome-mediated specificity in Hox mRNA translation and vertebrate tissue patterning. *Cell* 2011;145(3):383–397.
4. Narla A, Hurst SN, Ebert BL. Ribosome defects in disorders of erythropoiesis. *Int. J. Hematol.* 2011;93(2):144–149.
5. Horos R et al. Ribosomal deficiencies in Diamond-Blackfan anemia impair translation of transcripts essential for differentiation of murine and human erythroblasts. *Blood* 2012;119(1):262–272.
6. Ludwig LS et al. Altered translation of GATA1 in Diamond-Blackfan anemia. *Nat. Med.* 2014;20(7):748–753.
7. Dickson KA, Haigis MC, Raines RT. Ribonuclease inhibitor: structure and function. *Prog. Nucleic Acid Res. Mol. Biol.* 2005;80:349–374.
8. Furia A et al. The ribonuclease/angiogenin inhibitor is also present in mitochondria and nuclei. *FEBS Lett.* 2011;585(4):613–617.
9. Kobe B, Deisenhofer J. A structural basis of the interactions between leucine-rich repeats and protein ligands. *Nature* 1995;374(6518):183–186.
10. Haigis MC, Haag ES, Raines RT. Evolution of ribonuclease inhibitor by exon duplication. *Mol. Biol. Evol.* 2002;19(6):959–963.
11. Dickson KA et al. Ribonuclease inhibitor regulates neovascularization by human angiogenin. *Biochemistry* 2009;48(18):3804–3806.
12. Monti DM, Montesano Gesualdi N, Matousek J, Esposito F, D'Alessio G. The cytosolic ribonuclease inhibitor contributes to intracellular redox homeostasis. *FEBS Lett.* 2007;581(5):930–934.
13. Monti DM, D'Alessio G. Cytosolic RNase inhibitor only affects RNases with intrinsic cytotoxicity. *J. Biol. Chem.* 2004;279(38):39195–39198.
14. Godin I, Cumano A. The hare and the tortoise: an embryonic haematopoietic race. *Nat. Rev. Immunol.* 2002;2(8):593–604.
15. Huber TL, Kouskoff V, Fehling HJ, Palis J, Keller G. Haemangioblast commitment is initiated in the primitive streak of the mouse embryo. *Nature* 2004;432(7017):625–630.

16. McGrath K, Palis J. Chapter 1 Ontogeny of Erythropoiesis in the Mammalian Embryo [Internet]. In: *Red Cell Development*. Elsevier; 2008:1–22
17. Baron MH, Isern J, Fraser ST. The embryonic origins of erythropoiesis in mammals. *Blood* [published online ahead of print: February 15, 2012]; doi:10.1182/blood-2012-01-153486
18. Fujiwara Y, Chang AN, Williams AM, Orkin SH. Functional overlap of GATA-1 and GATA-2 in primitive hematopoietic development. *Blood* 2004;103(2):583–585.
19. Fujiwara Y, Browne CP, Cunniff K, Goff SC, Orkin SH. Arrested development of embryonic red cell precursors in mouse embryos lacking transcription factor GATA-1. *Proc. Natl. Acad. Sci. U.S.A.* 1996;93(22):12355–12358.
20. Shivdasani RA, Mayer EL, Orkin SH. Absence of blood formation in mice lacking the T-cell leukaemia oncogene tal-1/SCL. *Nature* 1995;373(6513):432–434.
21. Moenner M, Vosoghi M, Ryazantsev S, Glitz DG. Ribonuclease inhibitor protein of human erythrocytes: characterization, loss of activity in response to oxidative stress, and association with Heinz bodies. *Blood Cells Mol. Dis.* 1998;24(2):149–164.
22. Ferkowicz MJ et al. CD41 expression defines the onset of primitive and definitive hematopoiesis in the murine embryo. *Development* 2003;130(18):4393–4403.
23. Bertrand JY et al. Characterization of purified intraembryonic hematopoietic stem cells as a tool to define their site of origin. *Proc. Natl. Acad. Sci. U.S.A.* 2005;102(1):134–139.
24. Lancrin C et al. The haemangioblast generates haematopoietic cells through a haemogenic endothelium stage. *Nature* 2009;457(7231):892–895.
25. Socolovsky M. Ineffective erythropoiesis in Stat5a^{-/-}5b^{-/-} mice due to decreased survival of early erythroblasts. *Blood* 2001;98(12):3261–3273.
26. Pevny L et al. Erythroid differentiation in chimaeric mice blocked by a targeted mutation in the gene for transcription factor GATA-1. *Nature* 1991;349(6306):257–260.
27. Sankaran VG et al. Exome sequencing identifies GATA1 mutations resulting in Diamond-Blackfan anemia. *J. Clin. Invest.* 2012;122(7):2439–2443.
28. Koefler HP, Golde DW. Human myeloid leukemia cell lines: a review. *Blood* 1980;56(3):344–350.
29. O'Brien KA et al. Molecular convergence in ex vivo models of Diamond-Blackfan anemia. *Blood* 2017;129(23):3111–3120.
30. Crossley M, Tsang AP, Bieker JJ, Orkin SH. Regulation of the erythroid Kruppel-like factor (EKLF) gene promoter by the erythroid transcription factor GATA-1. *J. Biol. Chem.* 1994;269(22):15440–15444.

31. Welch JJ et al. Global regulation of erythroid gene expression by transcription factor GATA-1. *Blood* 2004;104(10):3136–3147.
32. Dresios J et al. Cold stress-induced protein Rbm3 binds 60S ribosomal subunits, alters microRNA levels, and enhances global protein synthesis. *Proc. Natl. Acad. Sci. U.S.A.* 2005;102(6):1865–1870.
33. Reschke M et al. Characterization and analysis of the composition and dynamics of the mammalian riboproteome. *Cell Rep* 2013;4(6):1276–1287.
34. Narla A, Ebert BL. Ribosomopathies: human disorders of ribosome dysfunction. *Blood* 2010;115(16):3196–3205.
35. Haigis MC, Kurten EL, Raines RT. Ribonuclease inhibitor as an intracellular sentry. *Nucleic Acids Res.* 2003;31(3):1024–1032.
36. Allam R et al. Viral RNA and DNA trigger common antiviral responses in mesangial cells. *J. Am. Soc. Nephrol.* 2009;20(9):1986–1996.
37. Gautier L, Cope L, Bolstad BM, Irizarry RA. affy--analysis of Affymetrix GeneChip data at the probe level. [Internet]2004;20(3):307–315.
38. Breitling R, Armengaud P, Amtmann A, Herzyk P. Rank products: a simple, yet powerful, new method to detect differentially regulated genes in replicated microarray experiments. [Internet]2004;573(1-3):83–92.
39. Hannah R, Joshi A, Wilson NK, Kinston S, Göttgens B. A compendium of genome-wide hematopoietic transcription factor maps supports the identification of gene regulatory control mechanisms. [Internet]2011;39(5):531–541.
40. Subramanian A et al. Gene set enrichment analysis: a knowledge-based approach for interpreting genome-wide expression profiles. *Proc. Natl. Acad. Sci. U.S.A.* 2005;102(43):15545–15550.
41. Sanjana NE, Shalem O, Zhang F. Improved vectors and genome-wide libraries for CRISPR screening. *Nat. Methods* 2014;11(8):783–784.
42. Bagnis C, Bailly P, Chapel-Fernandes S. Using an EGFPmeter to Evaluate the Lentiviral Vector Production: Tricks and Traps. In: *Viral Applications of Green Fluorescent Protein*. Totowa, NJ: Humana Press; 2009:151–163
43. Kim D et al. TopHat2: accurate alignment of transcriptomes in the presence of insertions, deletions and gene fusions. *Genome Biol.* 2013;14(4):R36.
44. Anders S, Pyl PT, Huber W. HTSeq--a Python framework to work with high-throughput sequencing data. *Bioinformatics* 2015;31(2):166–169.
45. Love MI, Huber W, Anders S. Moderated estimation of fold change and dispersion for RNA-seq data with DESeq2. *Genome Biol.* 2014;15(12):31.
46. Simillion C, Liechti R, Lischer HEL, Ioannidis V, Bruggmann R. Avoiding the pitfalls of gene set enrichment analysis with SetRank. *BMC Bioinformatics*

2017;18(1):151.

47. Karp PD et al. Expansion of the BioCyc collection of pathway/genome databases to 160 genomes. *Nucleic Acids Res.* 2005;33(19):6083–6089.

48. Gene Ontology: tool for the unification of biology 2000;25(1):25–29.

49. Kanehisa M et al. Data, information, knowledge and principle: back to metabolism in KEGG. *Nucleic Acids Res.* 2014;42(Database issue):D199–205.

50. Schaefer CF et al. PID: the Pathway Interaction Database. *Nucleic Acids Res.* 2009;37(Database issue):D674–9.

51. Croft D et al. The Reactome pathway knowledgebase. *Nucleic Acids Res.* 2014;42(Database issue):D472–7.

52. Kelder T et al. WikiPathways: building research communities on biological pathways. *Nucleic Acids Res.* 2012;40(Database issue):D1301–7.

53. Park E-H, Zhang F, Warringer J, Sunnerhagen P, Hinnebusch AG. Depletion of eIF4G from yeast cells narrows the range of translational efficiencies genome-wide. *BMC Genomics* 2011 12:1 2011;12(1):68.

54. Lee FS, Vallee BL. Modular mutagenesis of human placental ribonuclease inhibitor, a protein with leucine-rich repeats. *Proc. Natl. Acad. Sci. U.S.A.* 1990;87(5):1879–1883.

55. Wilm M et al. Femtomole sequencing of proteins from polyacrylamide gels by nano-electrospray mass spectrometry. *Nature* 1996;379(6564):466–469.

56. Huang DW, Sherman BT, Lempicki RA. Systematic and integrative analysis of large gene lists using DAVID bioinformatics resources. *Nat Protoc* 2009;4(1):44–57.

57. Huang DW, Sherman BT, Lempicki RA. Bioinformatics enrichment tools: paths toward the comprehensive functional analysis of large gene lists. *Nucleic Acids Res.* 2009;37(1):1–13.

58. Breitkreutz B-J, Stark C, Tyers M. Osprey: a network visualization system. *Genome Biol.* 2003;4(3):R22.

59. Giani FC et al. Targeted Application of Human Genetic Variation Can Improve Red Blood Cell Production from Stem Cells. *Cell Stem Cell* 2016;18(1):73–78.

60. Gupta D, Shah HP, Malu K, Berliner N, Gaines P. Differentiation and characterization of myeloid cells. *Curr Protoc Immunol* 2014;104:Unit 22F.5.–22F.5.28.

MAIN FIGURES

Figure. 1

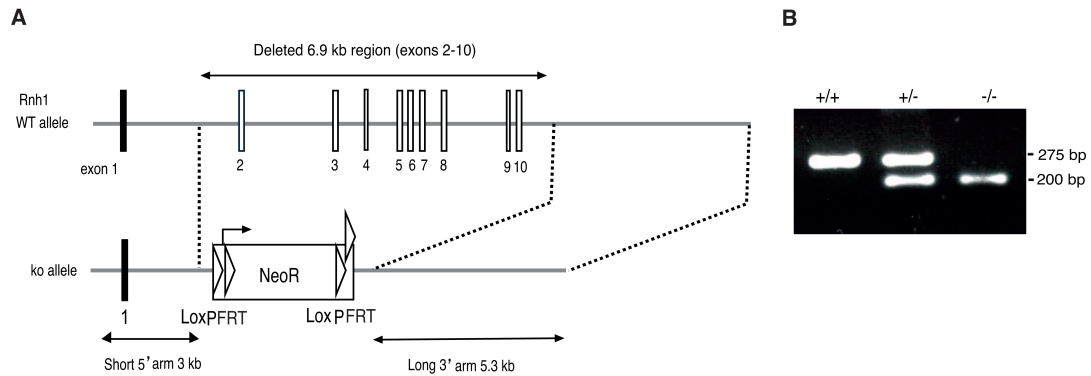


Figure 1. Generation of *Rnh1*^{-/-} mice.

(A) A 15.1 kb region used to construct the targeting vector was first subcloned from a positively identified C57BL/6 (RP23:210J2) BAC clone using a homologous recombination-based technique. The region was designed such that the long homology arm (LA) extended 5.30 kb 3' to exon 10. The short homology arm (SA) is located on the 5' side of exon 2 and is 2.96 Kb long. The Neo cassette replaces 6.89 kb of the gene, including exons 2-10. (B) DNA isolated from mouse embryos was genotyped by PCR. Primers were designed to distinguish wild type and neo cassette gene sequence. 275 bp size corresponds to wild type and 200 bp size corresponds to knock out mice.

Figure.2

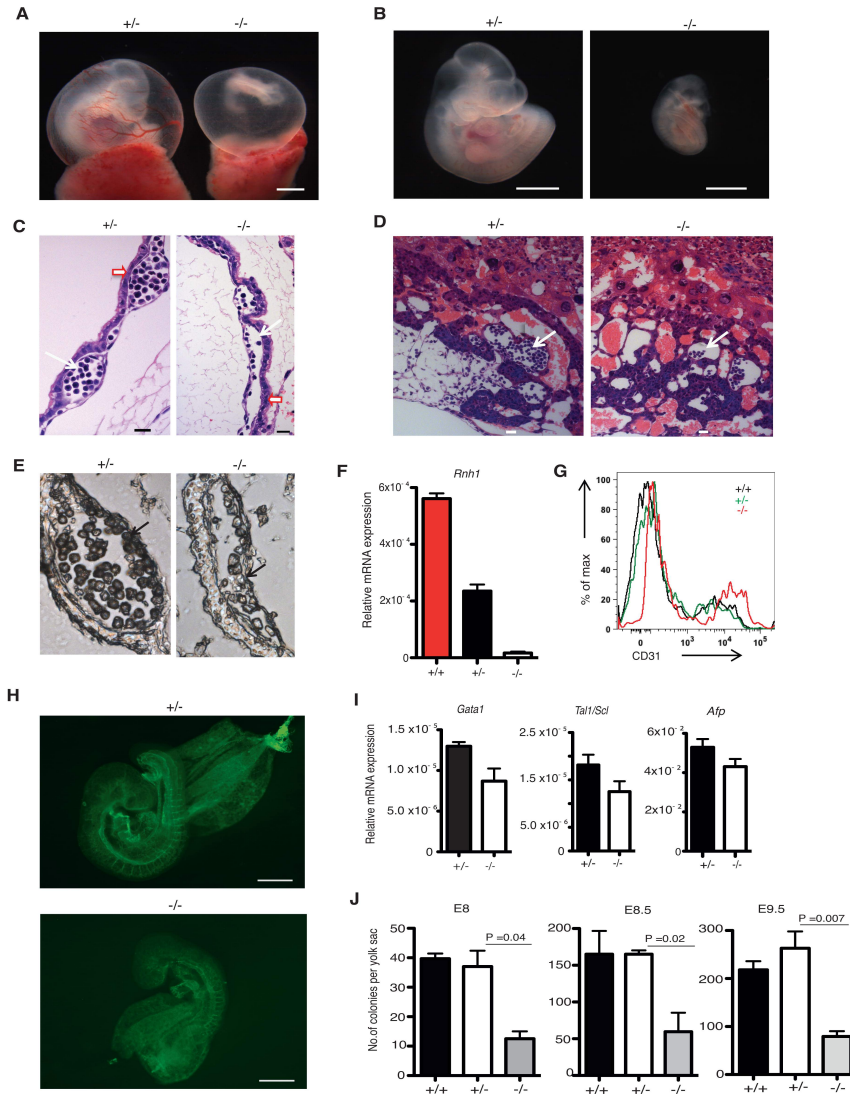


Figure 2. Decreased embryonic erythropoiesis in *Rnh1*-deficient mice

(A and B) Morphology of E10 *Rnh1*^{+/-} and *Rnh1*^{-/-} whole embryos (A) and embryo proper (B) (scale bar 1mm). (C) H&E stained sections through visceral yolk sac of *Rnh1*^{+/-} and *Rnh1*^{-/-} (scale bar 20 μm). Arrows indicate blood cells (thin), endothelium layer (thick). (D) Parasagittal section of placenta of *Rnh1*^{+/-} and *Rnh1*^{-/-} (scale bar 20 μm). Arrows indicate blood cells. (E) Benzidine-stained sections through visceral yolk sac of *Rnh1*^{+/-} and *Rnh1*^{-/-}. (F) qRT-PCR analysis of E9.5 yolk sac for *Rnh1*, normalized to 18S rRNA expression (n = 3-5). Data are means ±SEM. (G) CD31 mean fluorescence intensity analysed by flow cytometry (n=3) on E9.5 total yolk sac cells. (H) Pecam-1 (CD31) immunostaining of E9.5 *Rnh1*^{+/-} and *Rnh1*^{-/-} embryos (scale bar 500 μm). (I) qRT-PCR analysis on E9.5 yolk sac for the indicated mRNAs, normalized to 18S rRNA expression (n = 3-5). Data are means ±SEM. (J) Total number of colonies observed when E8- E9.5 yolk sac cells were cultured for 7 days in methyl cellulose medium (n = 3-4). Data are means ±SEM. *P* values determined by two-tailed *t*-test.

Figure 3

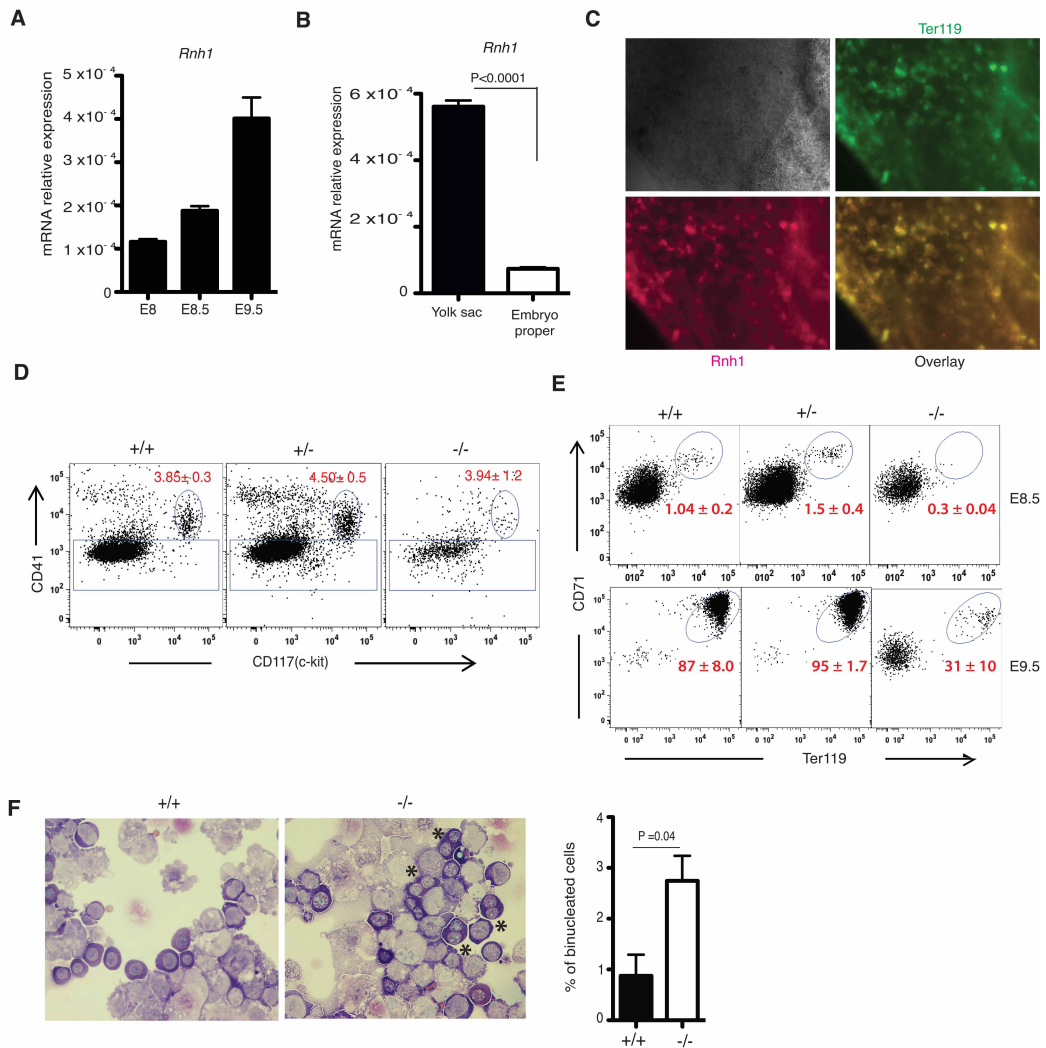


Figure 3. *Rnh1* expressed in embryonic erythropoiesis and regulates erythroid differentiation

(A and B) qRT-PCR analysis for *Rnh1* on whole embryos from different embryonic days as shown (A) and E9.5 yolk sac and embryo proper (B). mRNA levels are normalized to 18S rRNA expression (n = 3-4). Data are means ±SEM. (C) Immunostaining of a wild type E10.5 Yolk sac with RNH1 and the erythroid marker TER119. (D) Flow cytometry analysis for HSPCs on E9.5 yolk sac cells (n = 3-4). (E) Flow cytometry analysis for CD31-negative erythroid cells on E8.5 and E9.5 yolk sacs cells (n = 3-4). Data are means ±SEM. (F) Cytopspins from yolk sac cells were stained with Pappenheim stain (left). Binucleated erythroblasts are indicated by asterisks. Representative bar graph showing percentage of binucleated cells (right) (n=3). Data are means ±SEM. *P* values determined by two-tailed *t*-test.

Figure.4

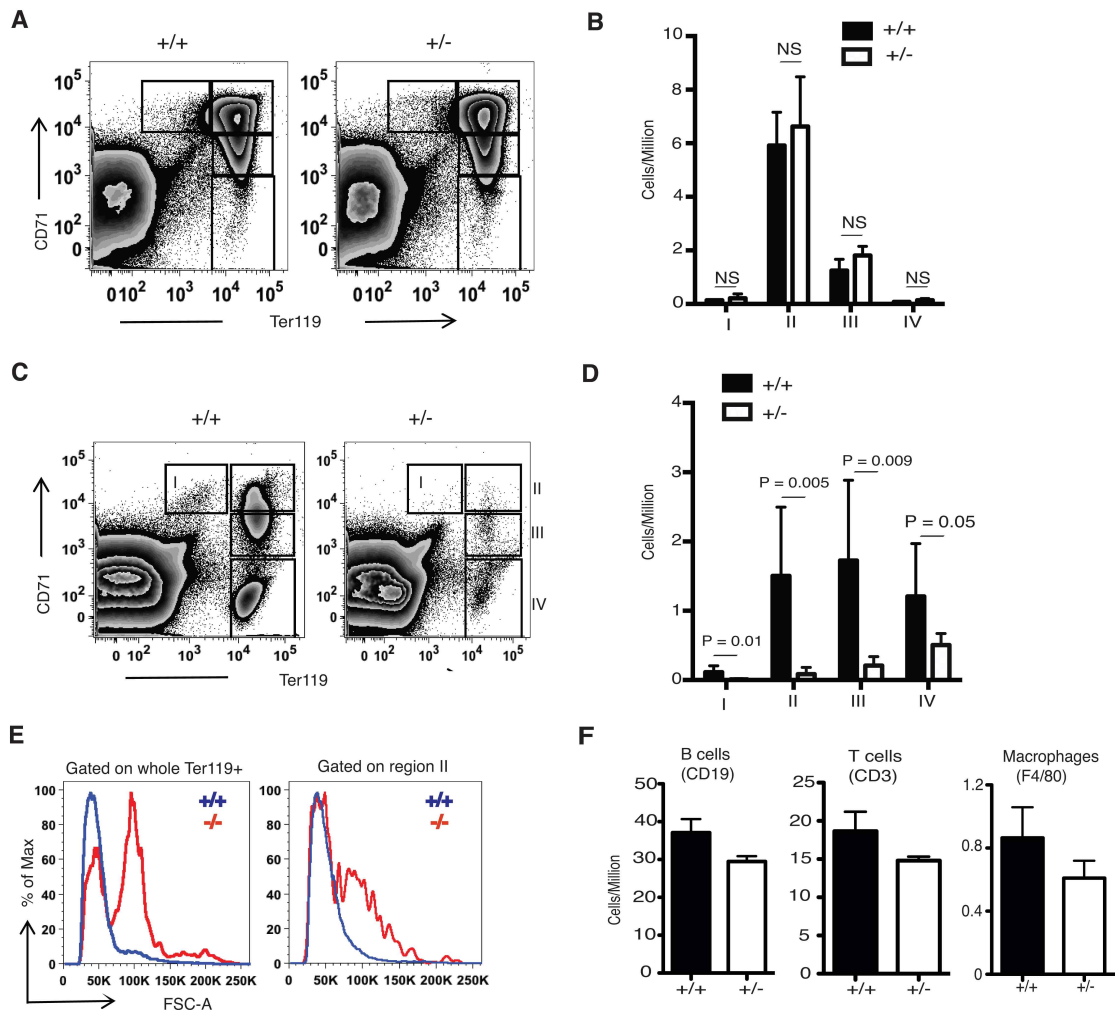


Figure 4. Decreased splenic erythropoiesis in *Rnh1*^{+/-} adult mice

(A and B) Flow cytometry analysis for erythroid cells of 8 weeks-old *Rnh1*^{+/-} and *Rnh1*^{+/+} mice bone marrow. (n = 6 mice). (C and D) Flow cytometry analysis for erythroid cells of 8 weeks-old *Rnh1*^{+/-} and *Rnh1*^{+/+} mice spleen (n = 6 mice). Different erythroblast subpopulations were selected as indicated I to IV. (I) proerythroblasts (II) basophilic erythroblasts (III) late basophilic and chromatophilic erythroblasts (IV) orthochromatophilic erythroblasts. Data are means \pm SD. (E) Flow cytometry forward-scatter distribution histograms of *Rnh1*^{+/-} and *Rnh1*^{+/+} mice spleen erythroid cells gated on total Ter119⁺ cells (Left) and on region II (Right). Data are means \pm SD. (F) Flow cytometry analysis for lymphoid and myeloid population on 8 weeks-old *Rnh1*^{+/-} and *Rnh1*^{+/+} mice spleen B cells, T cells and macrophages. (N = 6 mice). Data are means \pm SEM. *P* values determined by two-tailed *t*-test.

Figure.5

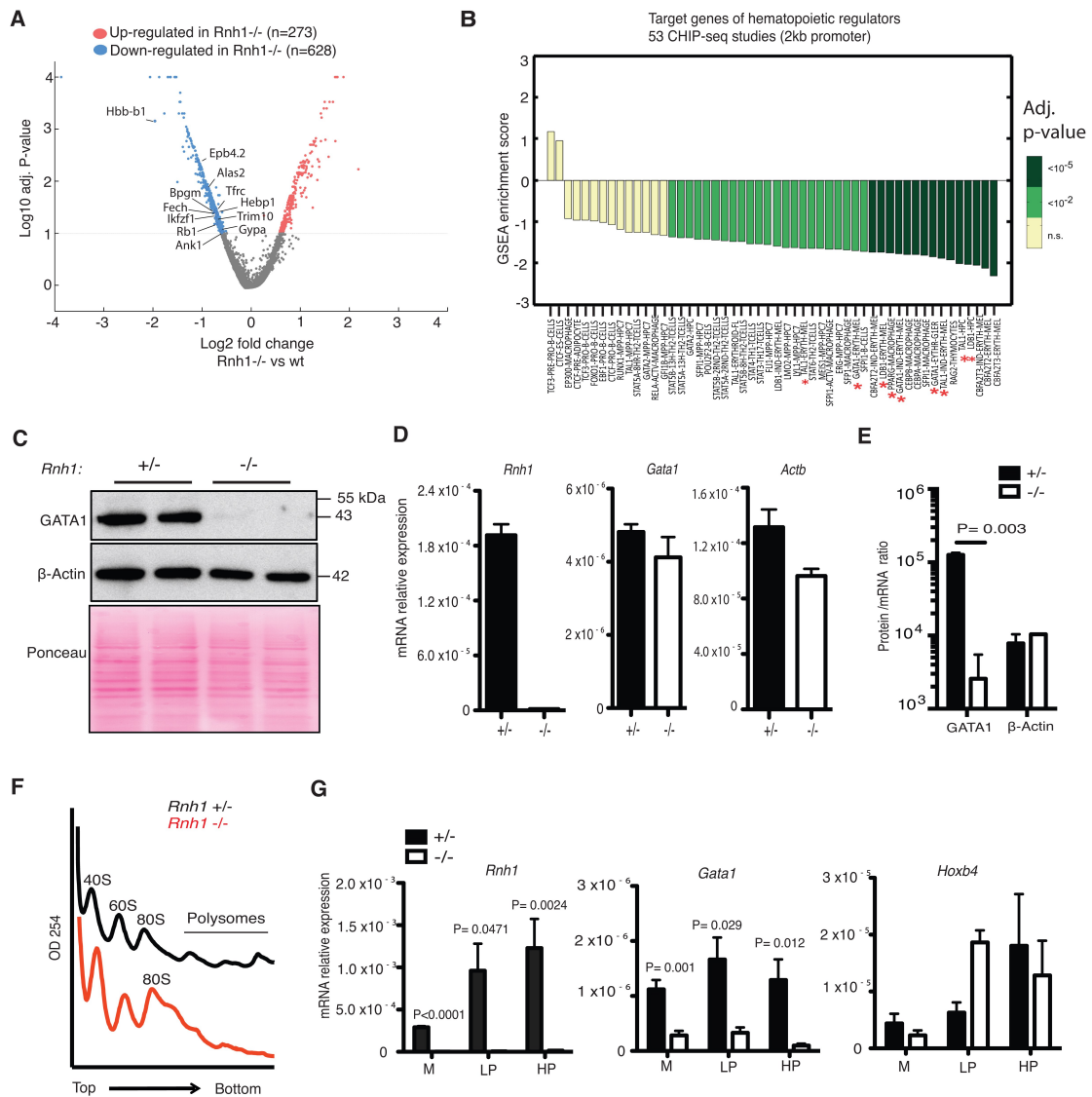


Figure 5. RNH1 deficiency decreases GATA1 protein levels

(A) Up and down regulated genes of E9.5 yolk sacs from *Rnh1*^{-/-} mice compared to wt (probability of false positive <0.1). (B) Target enrichment analysis of essential erythroid transcription factor targets in E9.5 yolk sacs from *Rnh1*^{-/-} mice. Bars correspond to the GSEA normalized enrichment scores of target sets extracted from a collection of ChIP-seq studies (n=52). n.s. corresponds to an adjusted p-value > 0.01. * indicates key regulators of erythropoiesis (C) Western blot analysis of total protein lysates isolated from E10 embryos, using indicated antibodies. Nitrocellulose membranes were stained with Ponceau S to demonstrate protein loading. Blots are representative of three independent experiments. (D) qRT-PCR analysis of E10 embryos for indicated mRNAs, normalized to 18S rRNA (n = 3). Data are means ±SEM. (E) Protein/mRNA ratios were determined using densitometric values of proteins, and 18S rRNA-normalized mRNA expression values for E10 total embryos. Data are expressed as mean ± SD. (F) Sucrose gradient polysome profiles for *Rnh1*^{+/+} and *Rnh1*^{-/-} yolk sac-derived cells from E10 embryos. The arrow shows the direction

of the sucrose gradient from low to high density. Data are representative of three independent experiments. (G) qRT-PCR analysis for indicated mRNAs in monosome (M), light polysome (LP) and heavy polysome (HP) fractions derived from E10 *Rnh1*^{+/-} and *Rnh1*^{-/-} yolk sac cells mRNA levels were normalized to 18S rRNA expression. Data are means ±SEM. Data are representative of three independent experiments. *P* values determined by two-tailed *t*-test.

Figure.6

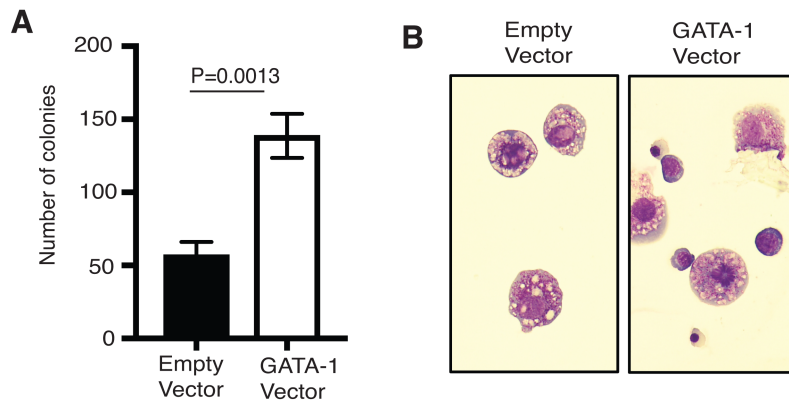


Figure 6. GATA1 overexpression rescue erythroid phenotype in Rnh1-deficient yolk sac cells

(A) Total number of colonies observed in control and GATA1- infected Rnh1-deficient yolk sac cells that were cultured for 7 days in methyl cellulose medium ($n = 3$). Data are means \pm SD. P values determined by two-tailed t -test. (B) Cytopsin images of erythroid cells derived from methyl cellulose colonies of control and GATA1- infected cells. More mature erythroid cells were observed in GATA1- infected cells.

Figure. 7

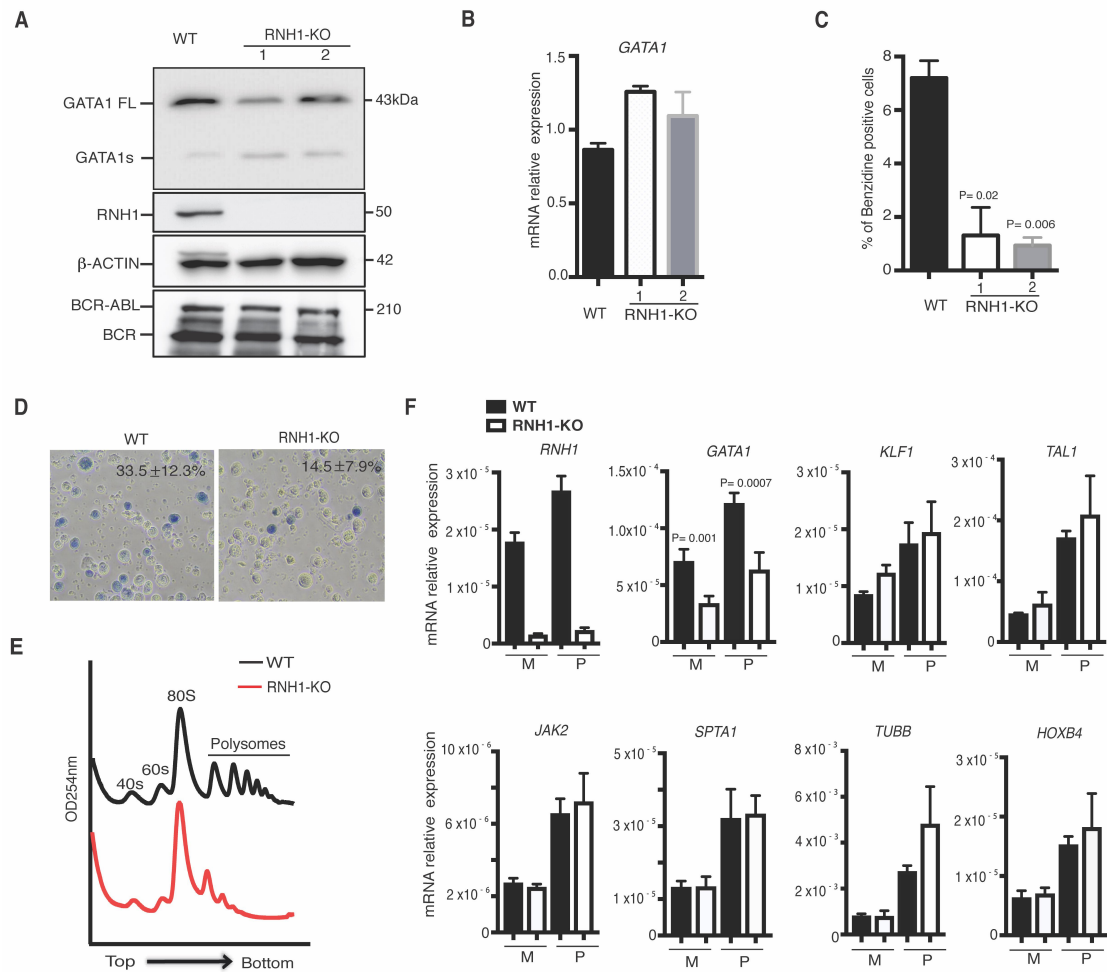


Figure 7. RNH1 deficiency decreases erythroid differentiation and GATA1 protein levels in K562 cell

(A) Total protein lysates of wild type and *RNH1*-KO K562 cells were analysed by Western blot with the indicated antibodies. K562 cells were positive for BCR-ABL oncogene. Blots are representative of three independent experiments. (B) qRT-PCR analysis for *GATA1* mRNA levels in K562 cells, normalized to 18S rRNA expression. Data are means \pm SD and representative of three independent experiments. (C) Number of benzidine-positive K562 cells. Data are means \pm SD and representative of three independent experiments. (D) K562 cells were treated with hemin (25 μ M) for 3 days and analysed for benzidine-positive cells. Data are means \pm SD and representative of three independent experiments. (E) Polysome profiles for WT and *RNH1*-KO K562 cells. Data are representative of three independent experiments. (F) qRT-PCR analysis for indicated mRNAs in monosome (M) and polysomes (P) fractions derived from WT and *RNH1*-KO K562 cells, normalized to 18S rRNA expression. Data are means \pm SD and are representative of three independent experiments. *P* values determined by two-tailed *t*-test.

Figure.8

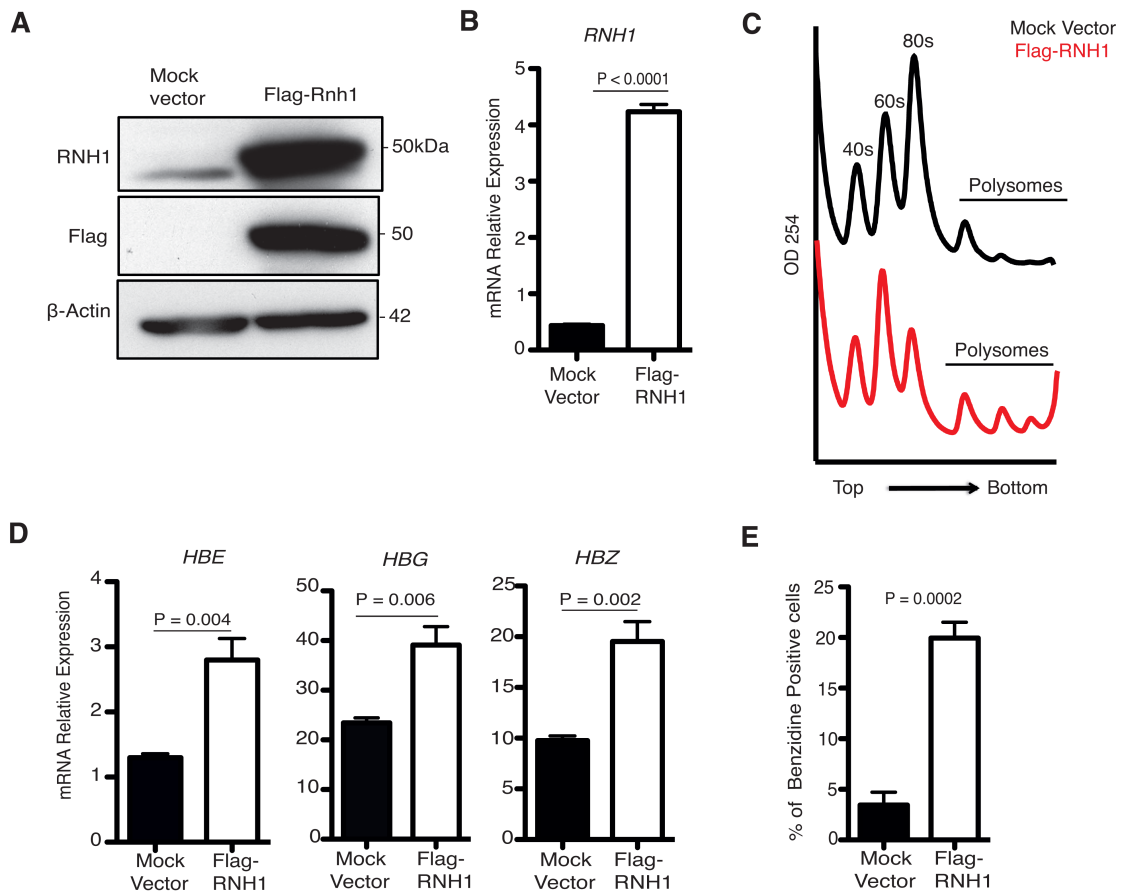


Figure 8. RNH1 induces globin gene expression in K562 cells

(A) RNH1 expression in stable K562 cells expressing mock or Flag-RNH1 vector by western blot. Blots were representative of two to three independent experiments. (B) RNH1 expression in stable K562 cells expressing mock or Flag-RNH1 vector by qRT-PCR. Data expressed mRNA relative expression normalized to HPRT expression. Data are means \pm SEM. Data were representative of three independent experiments. (C) Sucrose gradient polysome profiles for mock- or RNH1-expressing stable K562 cells. Arrows show direction of the sucrose gradient from less to more dense. Data are representative of three independent experiments. (D) qRT-PCR analysis for globin genes in stable K562 cells expressing mock or Flag-RNH1 vector. Data expressed mRNA levels normalized to HPRT expression. Data are means \pm SEM. (E) Percentage of benzidine positive cells in mock or Flag-RNH1 vector-expressing stable K562 cells. Data are means \pm SEM. Data were representative of three independent experiments. *P* values determined by two-tailed *t*-test.

Figure 9

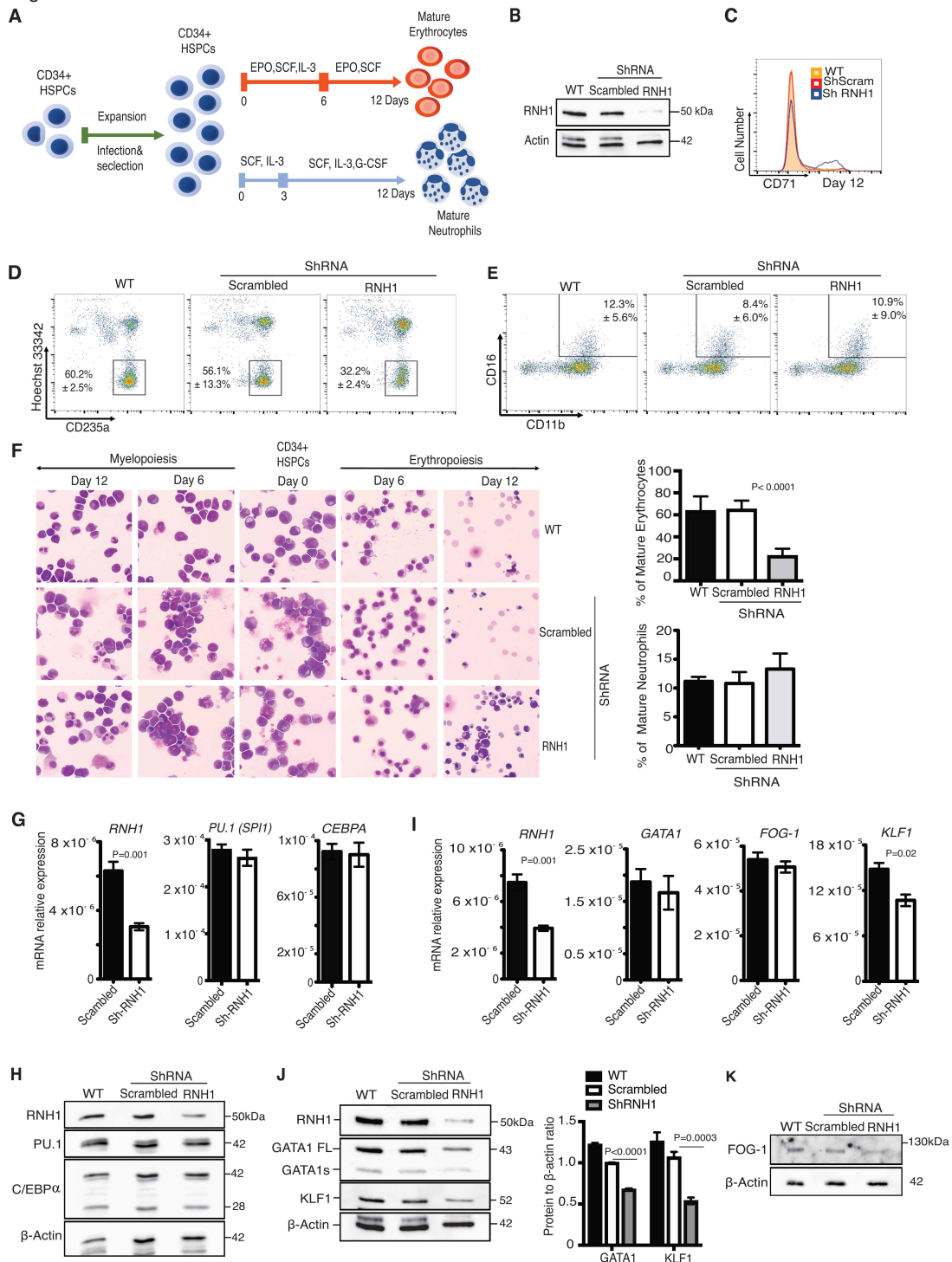


Figure 9. RNH1 knock down decreases GATA1 protein levels and erythroid differentiation in primary human CD34+ HSPCs

(A) Schematic illustration showing differentiation of human CD34+ HSPCs into mature erythrocytes and neutrophils. (B) Western blot analysis of RNH1 in CD34+ HSPCs after 4 days of transduction. (C) Representative histogram plot showing CD71 surface expression on day 12 of erythroid differentiation (N=3). (D) Flow cytometry analysis for CD235a⁺ and Hoechst 33342⁻ erythrocytes on day 12 of differentiation (N=3). Data are means ±SD. (E) Flow cytometry analysis for CD11b⁺ and CD16⁺

neutrophils on day 12 of differentiation (N=3). Data are means \pm SD. **(F)** Cytospin images of erythroid (right) and myeloid (left) differentiated cells at the indicated days of differentiation, stained with May-Grünwald-Giemsa. Representative bar graph on the left showing percentage of morphologically mature erythrocytes (up) and mature neutrophils (down) at day 12 of differentiation (n=3). Data are means \pm SD. **(G)** qRT-PCR analysis for indicated mRNAs in scrambled and RNH1 knock down myeloid cells at day 6 of differentiation (N=3), normalized to 18S rRNA expression. Data are means \pm SD **(H)** Total protein lysates of scrambled and RNH1 knock down myeloid cells at day 6 of differentiation were analysed by western blot with the indicated antibodies. **(I)** qRT-PCR analysis for indicated mRNA expression in scrambled and RNH1 knock down erythroid cells at day 6 of differentiation (N=3), normalized to 18S rRNA expression. Data are means \pm SD **(J and K)** Total protein lysates of scrambled and RNH1 knock down erythroid cells at day 6 of differentiation were analysed by western blot with the indicated antibodies. Right side in figure **J**, densitometric analysis for proteins by Image J program. Values were normalized to β -Actin. Data were expressed as mean \pm SD (right). All Blots are representative of three independent experiments. *P* values determined by two-tailed *t*-test.

Figure. 10

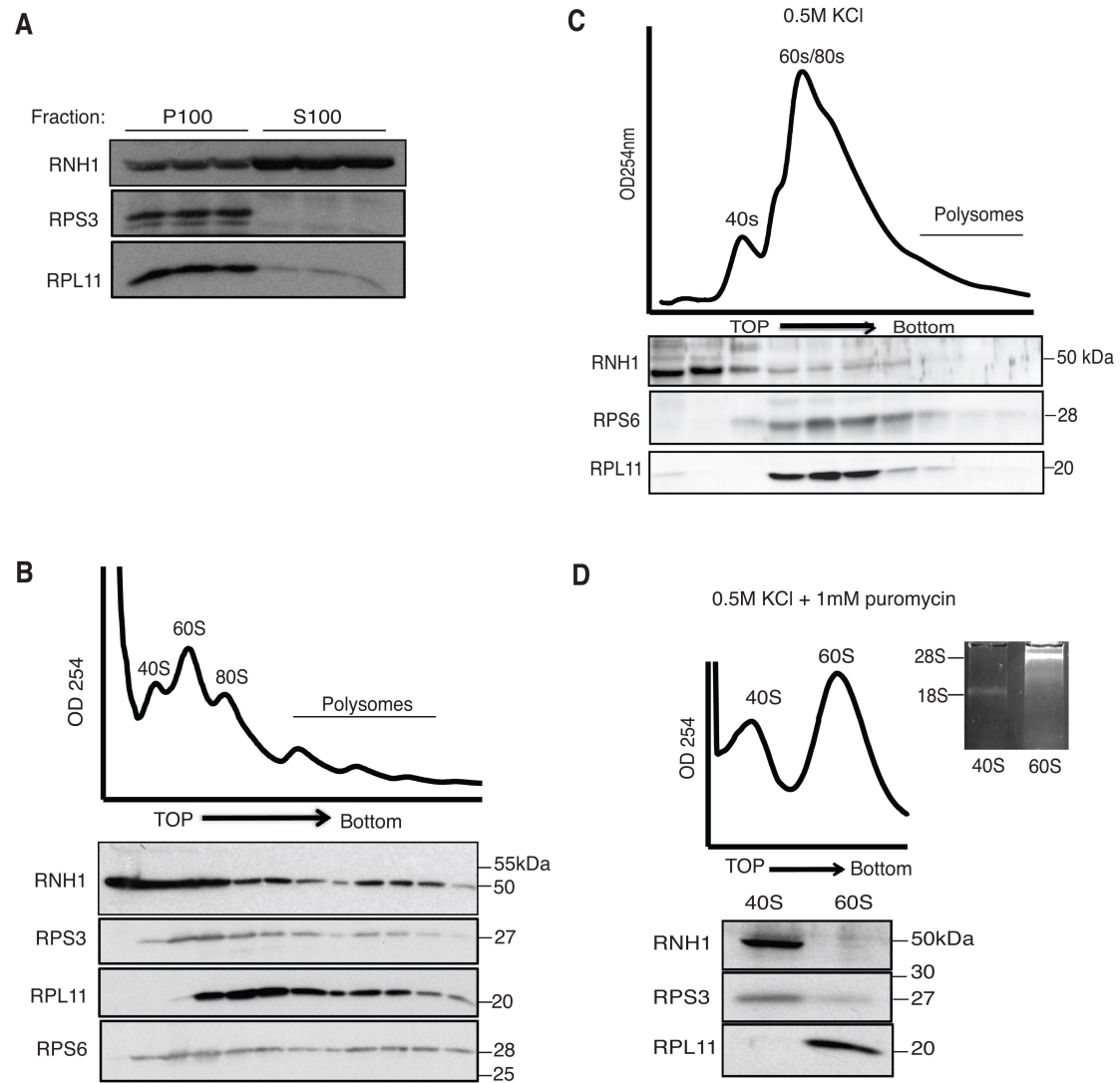


Figure 10. RNH1 is present in ribosomal fraction and binds to small ribosomal subunit

(A) Western blot analysis of RNH1 and ribosomal proteins in polysome-enriched pellet (P100) and the post-polysomal supernatant (S100) fraction prepared from K562 cytoplasmic extracts. Blots are representative of three independent experiments. (B) Western blot analysis of the distribution of RNH1 and ribosomal proteins in sucrose gradient polysome profile fractions prepared from K562 cell lysates. Blots are representative of three independent experiments. (C) Polysome-enriched fractions were treated with high salt conditions (0.5M KCl). Distribution of RNH1 and ribosomal proteins were analysed by western blot in sucrose gradient polysome profiles. Blots are representative of three independent experiments. (D) Polysome-enriched fractions were dissociated to 40S and 60S ribosomal subunits with puromycin. The distribution of RNH1 and ribosomal proteins in pooled fractions were analysed by western blot in sucrose gradient polysome profiles. Blots are representative of three independent experiments. 18S and 28S rRNA from pooled 40S and 60S fractions, were analysed to check the purity of the 40s and 60s subunits respectively.

Figure. 11

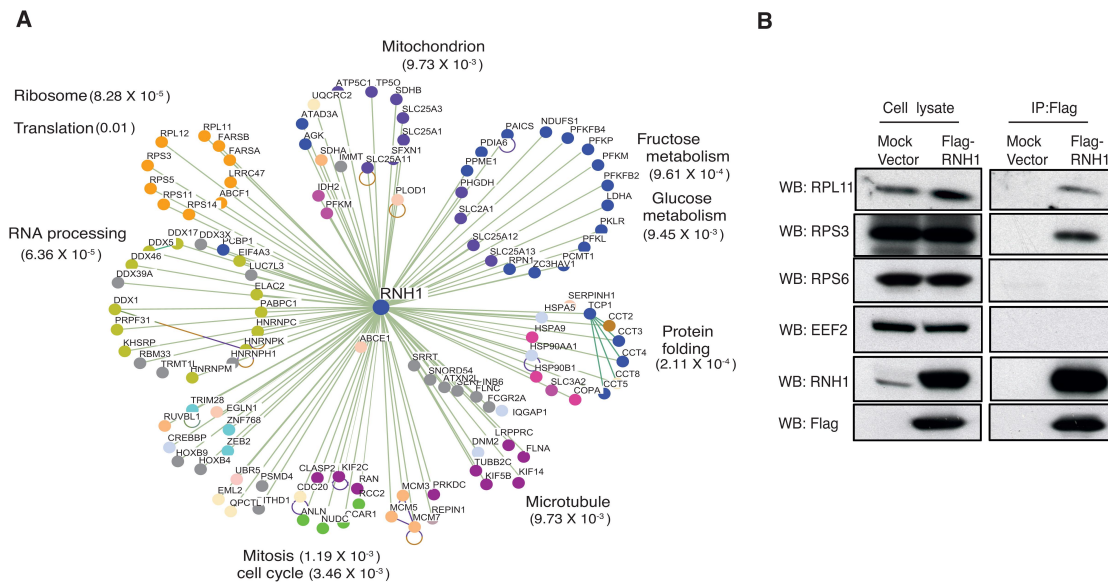


Figure 11. RNH1 binds to ribosomal proteins

(A) Functional enrichment analysis of RNH1 binding proteins identified by mass spectrometry (Benjamini-Hochberg adjusted P-values < 0.05). Protein interaction networks were visualized using Osprey. (B) Whole cell lysates of stable K562 cells expressing mock or Flag-RNH1 vectors (left) were used for anti-Flag immunoprecipitation and immunoblotting, as indicated (right). Blots are representative of three independent experiments.

Figure. 12

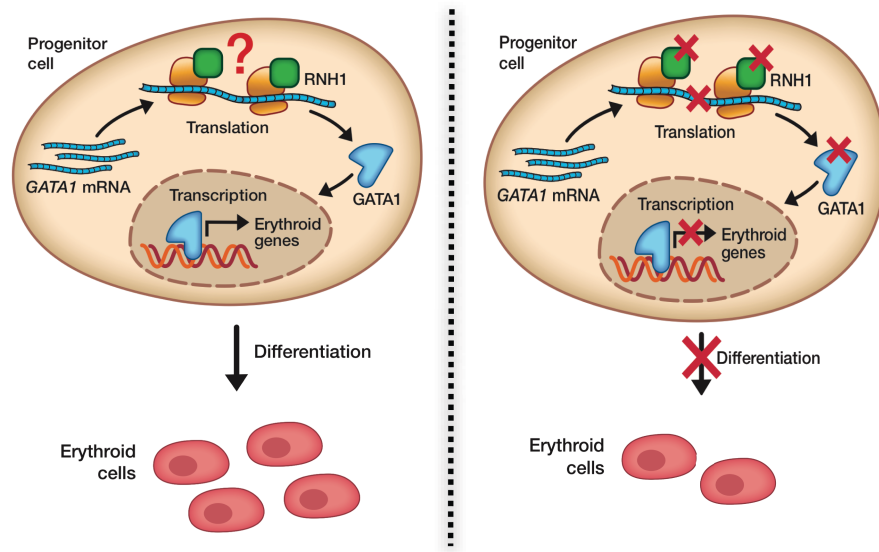


Figure 12. RNH1 is a ribosomal associated protein regulates erythropoiesis by controlling GATA1 translation

RNH1 is ribosomal associated protein involved in translation of GATA1, which leads to efficient differentiation of progenitor cells to mature erythroid cells. Lack of RNH1 decreases GATA1 levels, which leads to an arrest in differentiation.

Table. 1

Genotypes of Litters obtained by Intercrossing <i>Rnh1</i> ^{+/-}				
Stages	Number of Pups	+/+	+/-	-/-
E8.5	32	8	13	11 [#]
E9.5	78	22	35	21 [#]
E10.5	28	5	15	0 [*]
E11.5	16	5	11	0
Pups	228	77	151	0

[#] Abnormal compared to wildtype
^{*} All knockout embryos were degenerated and residual tissue can be found

Table 1. Genotype table

Rnh1 heterozygous (*Rnh1*^{+/-}) mice were intercrossed. Genotypes of offspring were determined at different gestational days or after birth, as shown.